THE SCATTERING OF LOW VELOCITY NEUTRAL PARTICLES: THE Cs → Ar AND Cs → N_2 INTERACTIONS

By

THOMAS COLE IMESON II

A DISSERTATION PRESENTED TO THE GRADUATE COUNCIL OF
THE UNIVERSITY OF FLORIDA
IN PARTIAL FULFILLMENT OF THE REQUIREMENTS FOR THE
DEGREE OF DOCTOR OF PHILOSOPHY

UNIVERSITY OF FLORIDA

December, 1965

ACKNOWLEDGMENT

The author wishes to express his appreciation to Dr. S. O. Colgate, Chairman of his supervisory committee, whose able assistance and guidance made this investigation possible, and to E. C. Whitehead for his assistance in the design and construction of the apparatus. He is also grateful to the members of his supervisory committee for their comments and suggestions concerning this dissertation. Finally, appreciation is extended to the Department of Health, Education and Welfare and the National Science Foundation for their support and financial assistance.

TABLE OF CONTENTS

LIST OF TABLES

LIST OF FIGURES

I. INTRODUCTION

All chemical and physical properties of matter in bulk are manifestations of the forces which exist between atoms. The various types of interactions between ions, atoms, and molecules in their ground states can be generally classed into those that act over short or long distances.[1] The short-range, or valance, forces arise from the interaction of electrons associated with the participating molecules;[2] they are repulsive and, as a rule, highly directional. Long-range interactions are attractive and usually less pronounced.

Forces between molecules at small distances are rather difficult to treat generally on a theoretical basis. Much that is known about them has come from calculations involving specific interactions. In most circumstances these forces are considered to vary exponentially with intermolecular separation. I. Amdur and co-workers,[3-5] using high energy molecular beam techniques, have conducted extensive investigations into the nature of short-range phenomena.

Long-range forces are usually divided into three categories: electrostatic, induction, and dispersion. An

inverse relationship to powers of the intermolecular separation can be attributed to all forms of these forces. Explanations of the first two types depend entirely on electrostatic principles; the basis for dispersion interactions, however, is found only in quantum mechanics.

Electrostatic forces constitute the simplest contribution to long-range interactions. These result from the interaction of electric moments which may be present in molecules.

Induction forces emanate from the interaction of a molecule possessing a permanent electric moment (ion, dipole, etc.) and another molecule. This interaction arises from the moments induced in one molecule by the permanent charge distribution in the other molecule. In all cases the force varies directly with the polarizability of the molecule in which the moment is induced.

Although the classical significance of dispersion forces[6] is not completely apparent from their quantum mechanical derivation, a plausible explanation based on the following reasoning has been offered. At any instant the electronic configuration of a molecule will be such as to generate an instantaneous dipole moment (although the molecule may be completely neutral). This instantaneous dipole will then induce a moment in an adjacent molecule thus giving rise to an attractive force between them. The

dispersion force then results from the instantaneous force of attraction averaged over all instantaneous electronic configurations of the molecule.

Several statistical theories have been developed which relate the intermolecular potential energy to various macroscopic properties of matter; these properties include: viral coefficients of the equation of state, Joule-Thomson coefficient, and low density transport effects. If the intermolecular potential energy for a system is known, then the macroscopic properties listed above can be calculated, or conversely a representative form of the potential may be obtained from these measured properties.

A problem arises in that detailed quantum mechanical calculations concerning the interaction potential can be made only for the simplest cases; namely, the interactions of H atoms, He atoms, and H_2 molecules.[7] This difficulty results from an inability to treat many-body systems with any degree of mathematical accuracy. Therefore, intermolecular potentials must generally be obtained experimentally.

The procedure for arriving at the potential involves choosing an arbitrary analytical form with adjustable parameters, then fitting this function to the experimental data in order to obtain the best fit. With the exception of mutual-diffusion coefficients for unlike molecules, the

macroscopic properties of matter listed above are rather insensitive to the type of potential form used. This fact results in potentials of quite different character appearing to fit the experimental data with more or less equal precision.[8] As can be seen a more sensitive technique is required for determination of the potential with appreciable accuracy.

In general a direct and, in principle, simple means of obtaining information concerning the intermolecular potential involves the technique of corpuscular beam scattering.[9] The unique suitability of beam experiments for investigation of particle interaction results from their production of controlled collisions.

A molecular beam can be defined as a stream of molecules in a highly evacuated region moving practically collision free in straight and almost parallel trajectories within the confines of the geometrically defined beam. A beam may be formed by effusive flow of particles through an orifice with subsequent definition by one or more other apertures in line with the first. A molecular beam apparatus, therefore, consists fundamentally of a source chamber or oven, a series of collinear slits to define the beam, and a detector.

The first molecular beam of neutral particles moving in straight lines with thermal velocities was generated in

the laboratory of L. Dunoyer.[10] The importance of molecular beams as a research tool was first recognized by O. Stern[11] in 1919. He used this technique to obtain the first direct measurement of the average velocity of silver atoms in the vapor state.

The utility of molecular beam scattering techniques in determining intermolecular potentials originates in the relationship between the potential and the angle through which the relative velocity vector of the colliding particles is turned during a collision. A number of investigations have been carried out using molecular beams to furnish information concerning interaction potentials.[12-17]

Massey and Mohr[18] were the first to give an approximate quantum mechanical relationship between the relative velocity dependent collision cross-section and the intermolecular potential. Experimentally the cross-section is determined by the attenuation of a molecular beam passing through a gas filled region. Factors effecting the attenuation of a molecular beam are: energy of the beam, molecular masses, temperature and density of the scattering gas, scattering path length, aperture of the detector, and the nature of the interaction between the beam and target particles.

Several difficulties arise in the determination of relative velocity dependent cross-sections in the low

velocity region. Because of the Maxwellian or near Maxwellian velocity distribution present in the beam source, all molecular beams have rather large velocity spreads (the exception being beams formed at low temperature). Thus for precise measurements some type of velocity selection is generally required. For this and other purposes a variety of velocity selector types has been developed. These include: gravitation deflection, diffraction from crystal gratings, mechanical selectors involving rotating slotted devices, and magnetic deflection.[19-29] The latter two types are those in general use at the present.

Scattering experiments conducted with velocity selected beams traversing a gas filled region require averaging over all velocities present in the scattering gas to arrive at the velocity dependent collision cross-section. A more precise determination of the cross-section may be obtained if this averaging is eliminated. This may be accomplished by the use of a second velocity selected beam intersecting the original one. In this way highly controlled pairwise collisions can be created.

Use of two velocity selectors creates two rather serious problems. The first concerns the reduction in intensity that must always accompany velocity selection. This problem can be dealt with by improving detection techniques and increasing the original beam intensity.[30,31]

The second problem results from use of two independent rotating slotted types of velocity selectors. When selectors of this type are used the transmitted beam is pulsed, and the pulses from the two beams should be phased in such a way that they arrive at the impact zone simultaneously. Of course the magnetic deflection type of velocity selector does not suffer from this difficulty, however, it is specific to particles that possess a magnetic moment. The phasing problem can be resolved by the use of a slotted rotating velocity selector which acts on both beams simultaneously. Design and development of velocity selectors of this type has progressed in various laboratories.[32] The development of a double beam velocity selector of practical geometry and proven reliability for molecular beam scattering experiments will be reported here.

II. EXPERIMENTAL

A. Apparatus

The molecular beam apparatus (Figure 1) to be described here allows the simultaneous velocity selection of two molecular beams. This selection technique facilitates production of highly controlled pairwise molecular collisions, thus allowing the interactions of atomic or molecular species to be investigated with a high degree of precision. The unique feature of this apparatus is the velocity selector; therefore it is appropriate to describe it before other aspects of the instrument are discussed.

1. Velocity selector

The trajectory of a point, moving with constant velocity v in the positive direction along the x axis, projected onto a coordinate system which is allowed to rotate about an axis through its origin with a constant angular speed ω is a spiral of Archimedes given by $|x| = r = v\theta/\omega$. A representation of this situation is shown in Figure 2. The trajectory is seen to be a function of the velocity and it is this fact which allows velocity selection to be effected. In order to fabricate a velocity selector, it is necessary to machine grooves on the surface of a

Fig. 1.-Photograph of apparatus during final stages of completion.

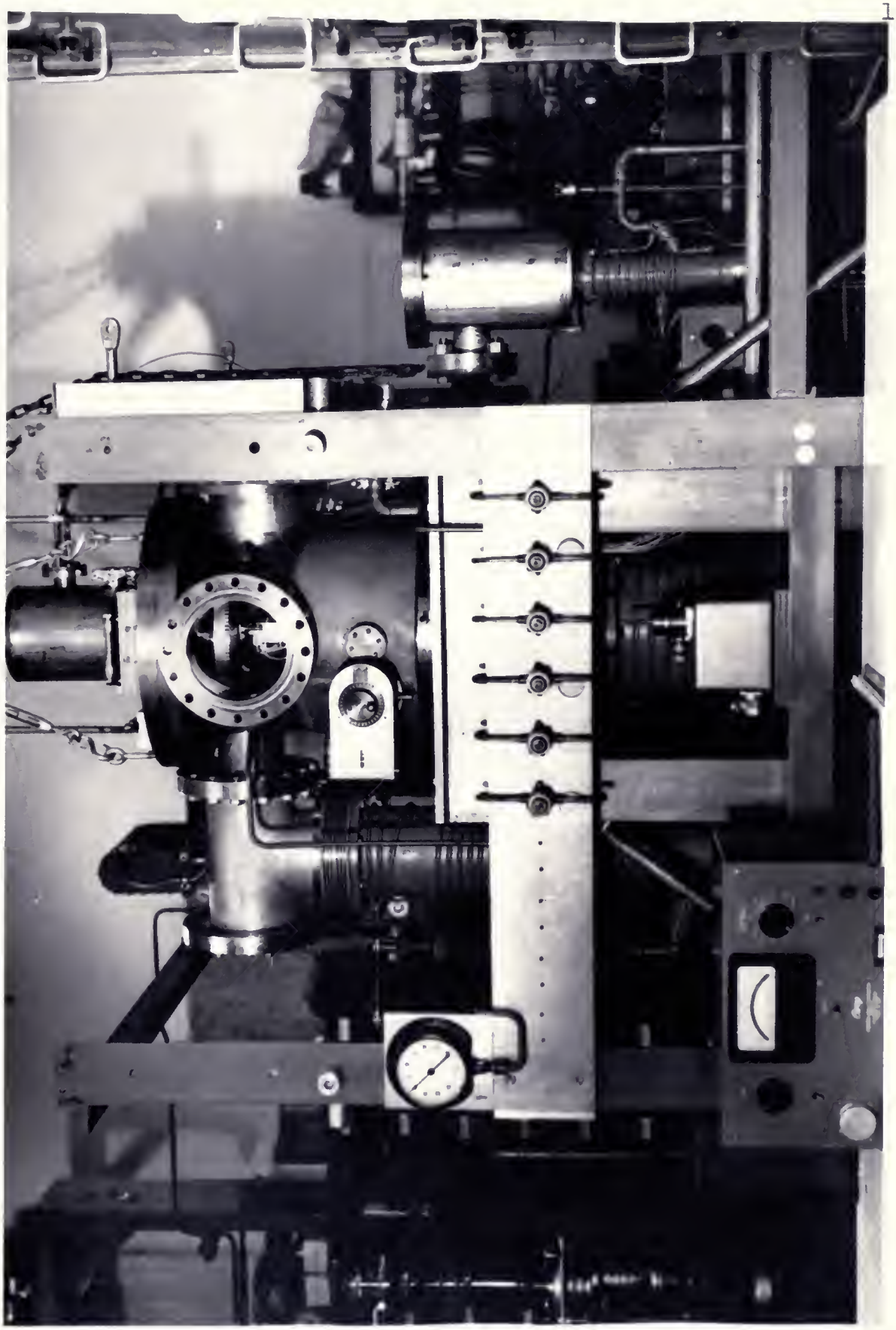

Fig. 2.-Trajectory of point moving with constant velocity v projected on plane rotating about the origin with angular velocity ω.

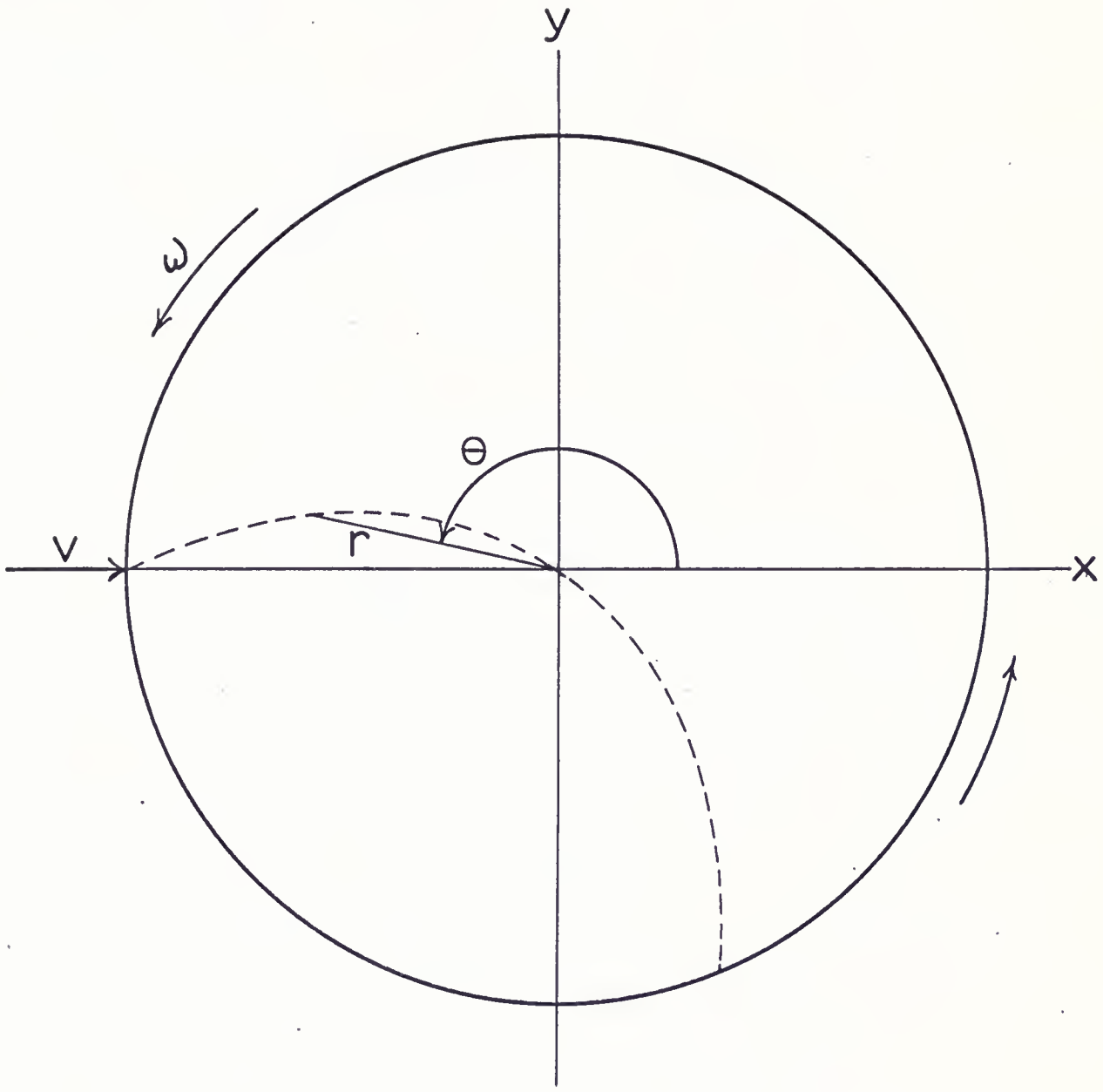
y
ω
θ
v
r
x

circular disk; the groove width being such as to accommodate only trajectories of a narrow band of velocities. The simultaneous velocity selection of two molecular beams is accomplished by positioning grooves in precise relationships to one another and directing the two beams through the selector so they intersect at the axis of rotation. Figure 3 illustrates the spacings (90°) between related grooves in the present selector.

For use in the first selector three different groove geometries (Figure 4) were considered with regard to ease of fabrication and transmission characteristics. The ideal groove subtends the same angle from the center of the selector at any position along the groove. It possesses excellent transmission characteristics but offers considerable difficulties in construction. The linear groove is the simplest to fabricate but possesses poor transmission properties. The parallel wall groove can be fabricated with some difficulty but has rather good transmission characteristics. It is for these reasons that the latter groove geometry was chosen.

The velocity selector was machined from a three inch thick 7075-T651 aluminum plate, ultrasonically tested for uniformity and furnished by the Aluminum Company of America. A 13 in. diameter rotor blank was cut whose over-all-thickness was 2.950 in. (Figure 5). After thorough testing as

Fig. 3.-Orientation of grooves for simultaneous velocity selection of perpendicular beams.

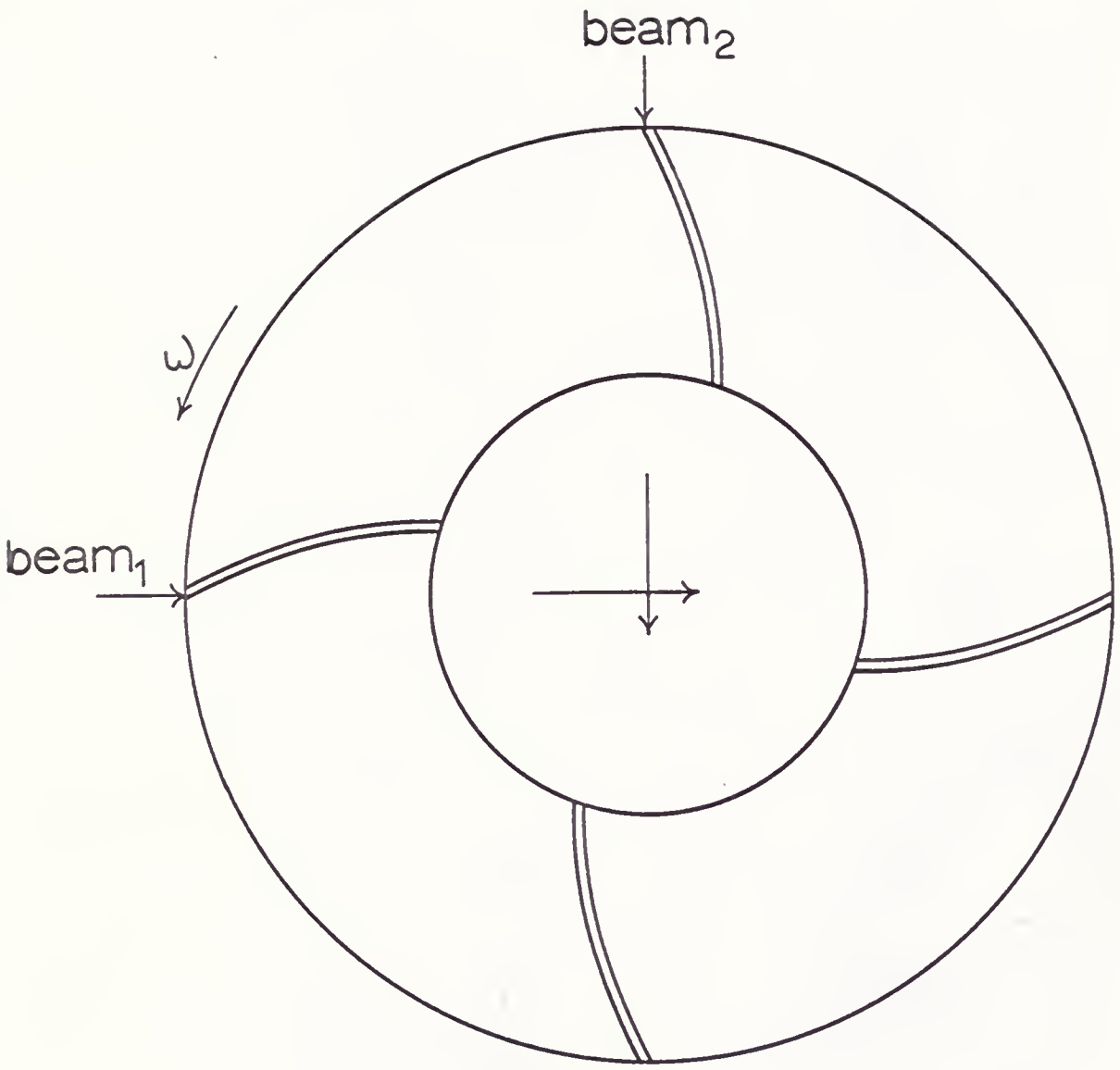
beam2
ω
beam1

Fig. 4.-Geometries of some possible velocity selecting grooves.

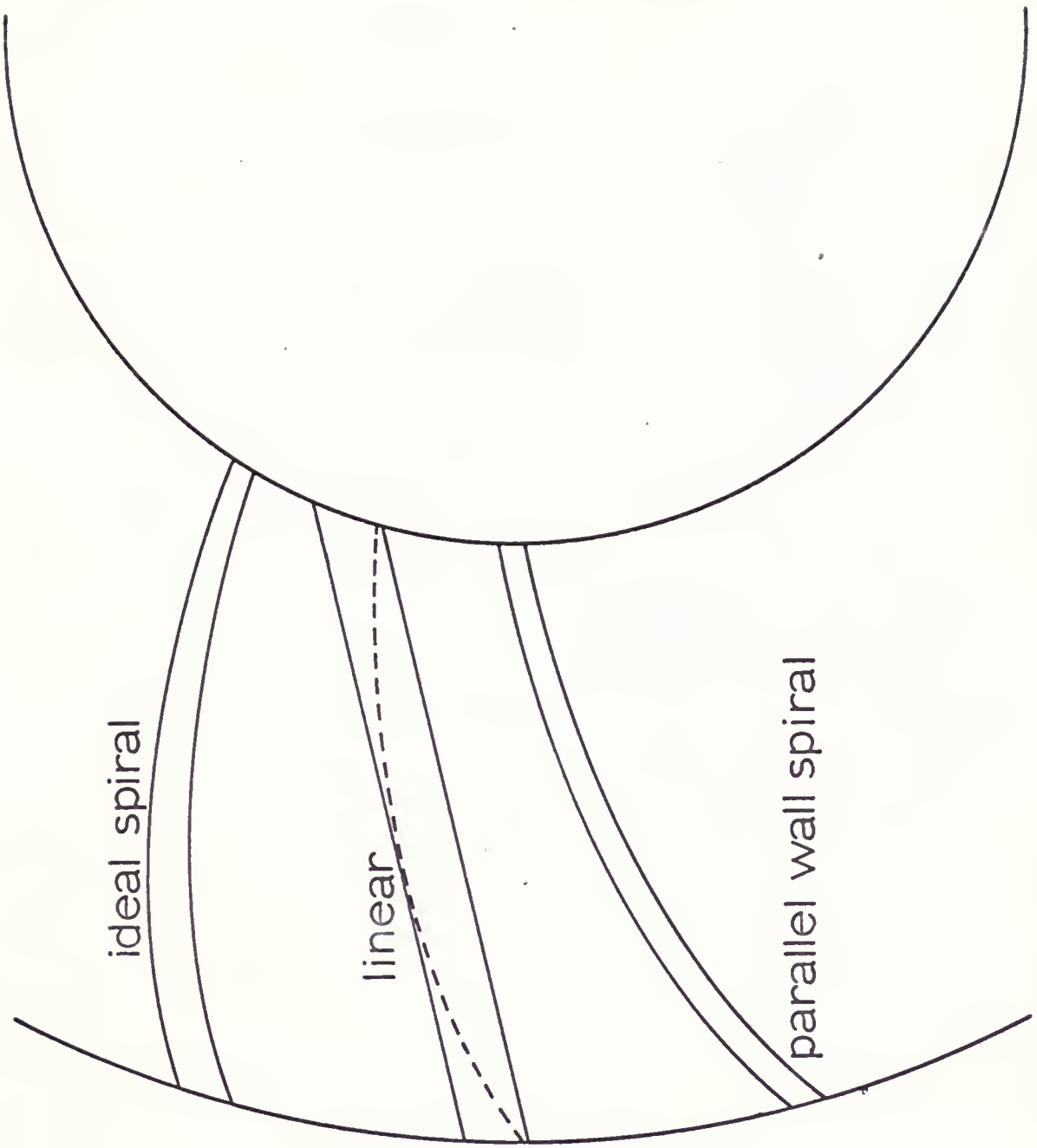
ideal spiral
linear
parallel wall spiral

Fig. 5.-Drawing of aluminum velocity selector showing geometry of the four linear optical alignment grooves.

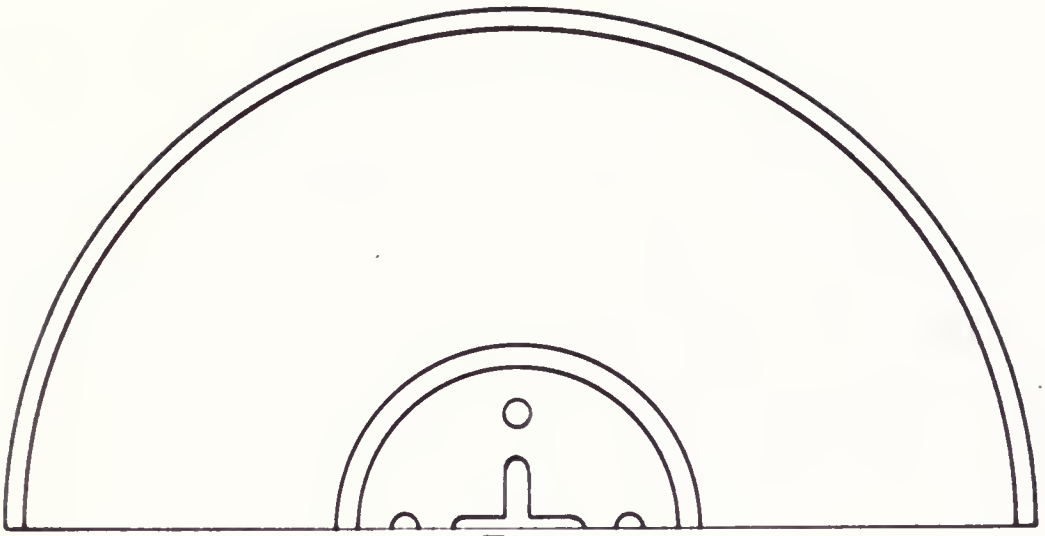

Top

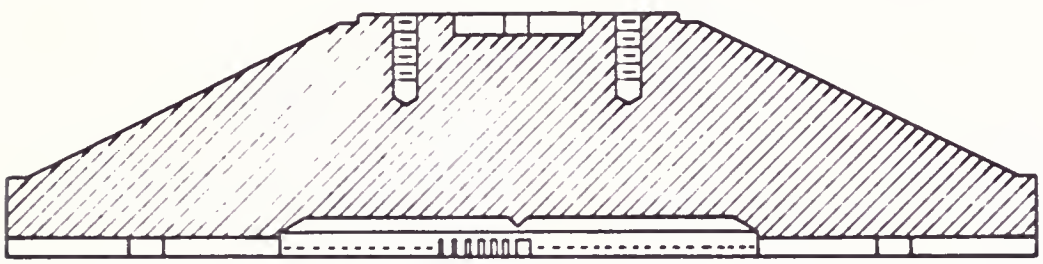

Profile

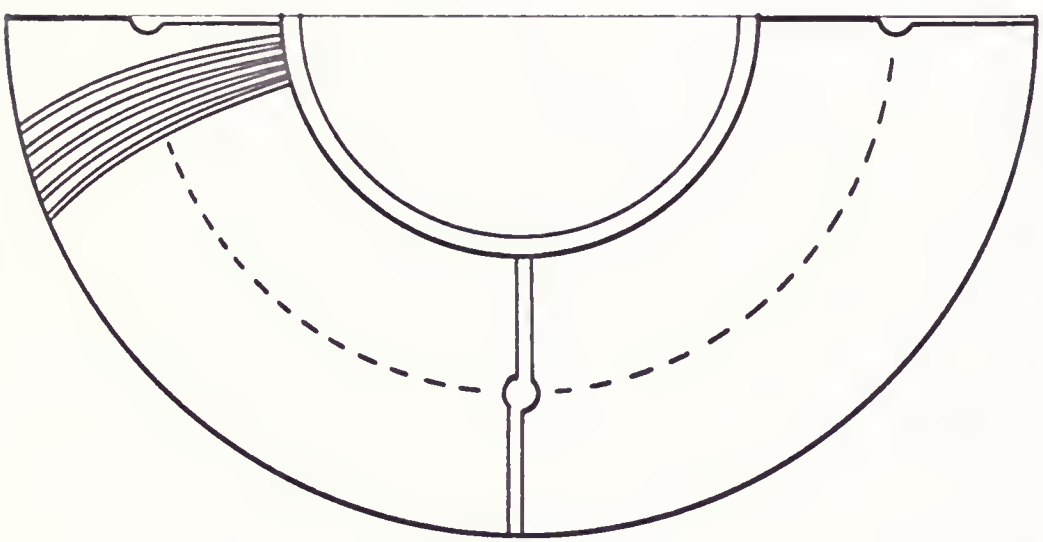

Bottom

to its dynamic and static balance the blank was prepared for grooving. The arrangement used to machine the grooves is shown in Figure 6. The step and four threaded holes at the top of the blank selector (Figure 5) were used to position and attach it to an indexing rotary table mounted concentrically on a Troyke rotary table which in turn was clamped to the table of a South Bend vertical milling machine. Rigid support of the rotary fixture was achieved by the use of a large thrust and double row ball bearing combination. One hundred sixty equally spaced positions were obtained by locating forty bored and reamed holes in the plate at the bottom of the fixture with four equally spaced indexing holes in an aluminum ring clamped to the rotary table. The handle of the commercial rotary table was replaced by a pinion which engaged a rack mounted on the longitudinal table of the milling machine. The grooves were cut with two-flute high speed steel end mills under a spray of kerosene from a high-pressure mist coolant system. The cutters were driven in a Precise high speed grinder miller mounted on the spindle of the milling machine. The spindle of the miller grinder was indicated into a position directly over the center of the system of rotary tables. With the rack and pinion engaged any linear motion of the transverse milling machine table caused the system of rotary tables to move through an angle proportional to the

Fig. 6.-Photograph of machine set-up for cutting parallel wall, spiral grooves.

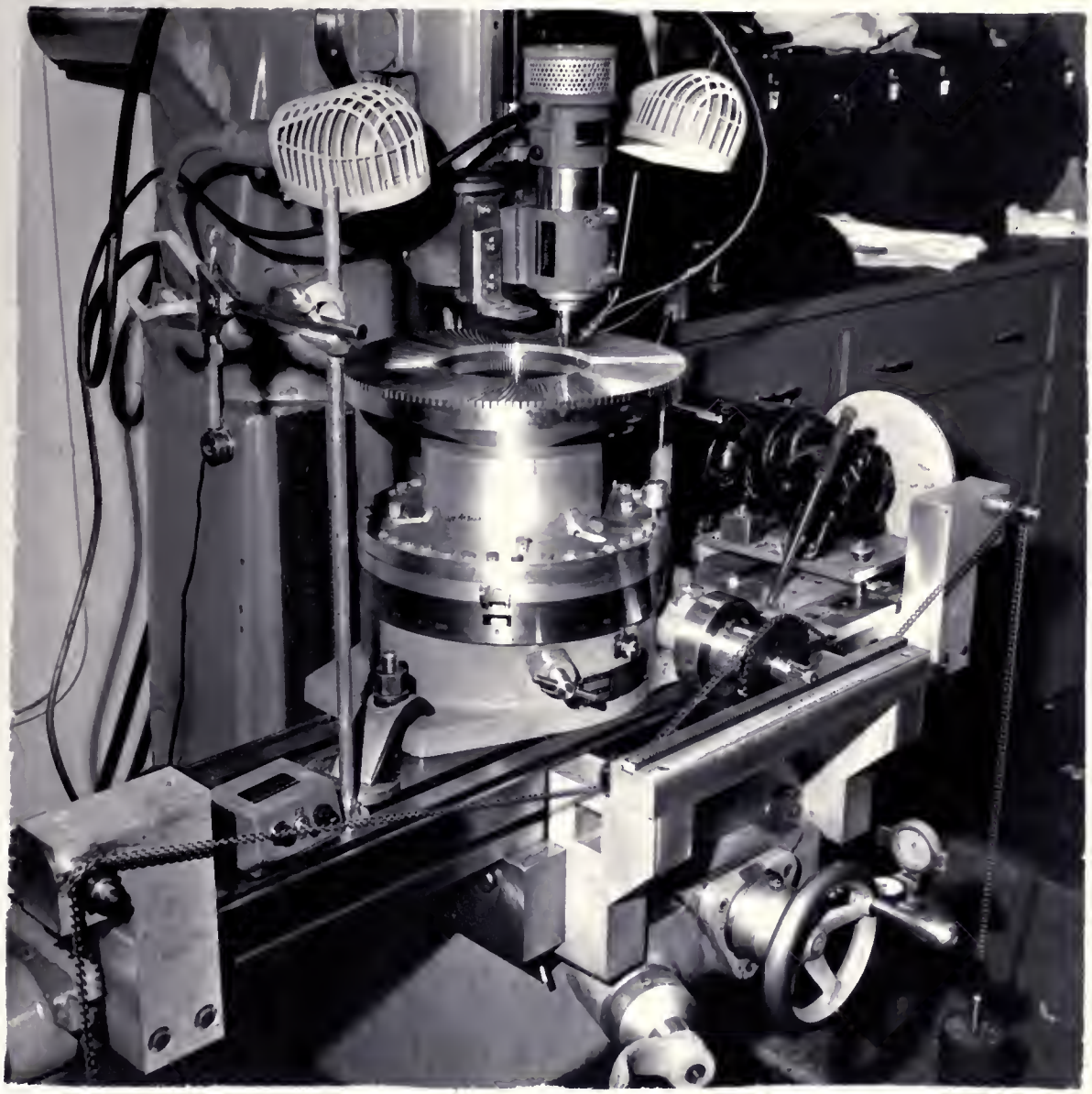

linear displacement, the proportionality being determined by the pitch diameter of the pinion gear. The path taken by the tool through the velocity selector, mounted in the prescribed arrangement, is a spiral of the desired type.

With the grinder miller running at a speed of 36,000 RPM the grooves were cut to a depth of 0.245 in. (in five steps) and a width of 0.055 in. A finishing cut was taken on each groove with a 0.069 in. diameter tool set at a depth of 0.250 in. The roughing and finishing operations, although conducted separately, were carried out on a particular groove and then on the groove diametric to it. This procedure assures that minimum imbalance is imparted to the selector by tool wear. Upon completion of the grooving operation the pinion was decoupled from the rack to allow machining of four straight optical alignment grooves (Figure 5). To give the straight grooves an effective slit width of .010 in., a 0.125 in. diameter end mill, offset from the center by 0.0575 in., was used to machine half the groove length with the remaining half being cut after offsetting the tool the same distance from center in the opposite direction. By means of these grooves the beam sources were set to perpendicularity. A total of 148 spiral grooves were cut in the selector, twelve grooves (three in each quadrant) were omitted to avoid their intersection with the straight grooves.

The device through which the velocity selector is coupled to its drive motor[33] (Figure 7) allows the selector to be suspended by means of a flexible shaft directly from the vertical shaft of the motor. The flexible shaft makes it unnecessary to perform the difficult task of dynamically balancing the coupled rotor. The drive bushing D, constructed of 304 stainless steel, has an outside nonretaining taper which matches exactly the inside taper of the 303 stainless steel cap C. This taper effects accurate positioning of the drive bushing; application of torque is through four cleats on the bottom of D which fit into slots milled in the top of the velocity selector (Figure 5). The flexible shaft F is machined from a single length of 304 stainless steel. Its lower end is shrunk fit into the central bored hole in D and welded at W. The upper portion of F threads loosely into RH 10-32 internal threads in the motor shaft. Both F and S have matching 60° tapers which position the shaft F so that it is precisely concentric with the motor shaft. The selector is driven clockwise; consequently positive positioning of F with respect to S is continually maintained. However, a LH 1/2 - 20 lock nut N is provided to bind the flexible shaft against a precision lock washer L to insure against loosening of the internal threads (particularly during deceleration). The diameter of the present flexible shaft is 0.100 in. and its exposed length is 1.5 in.

Fig. 7.-Diagram of velocity selector suspension system: S-drive motor shaft; N-left-hand lock nut; L-lock washer; F-flexible shaft; B-taper head bolt; D-tapered drive bushing; W-point where shaft is welded to drive bushing; C-stainless steel cap.

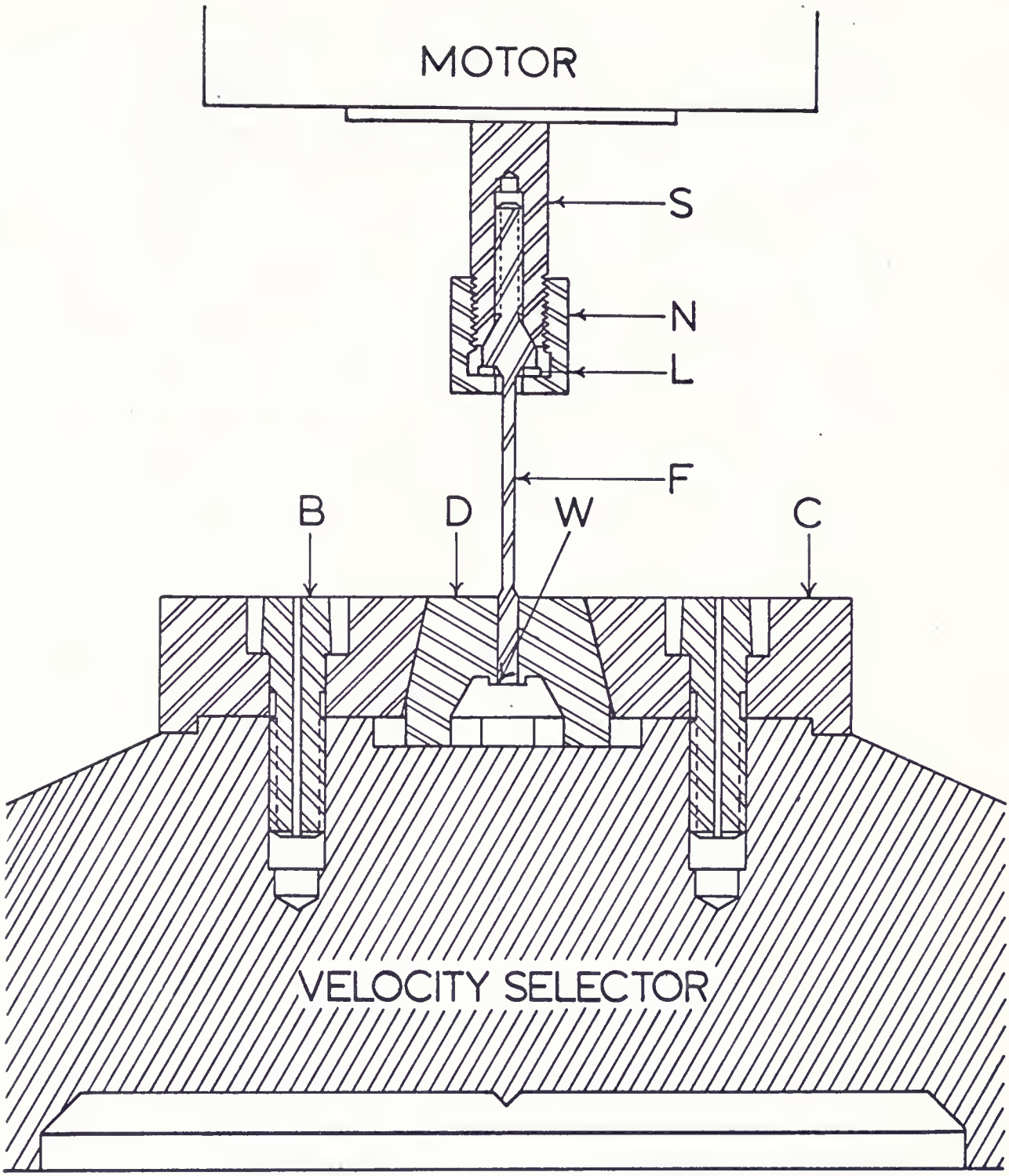
MOTOR
S
N
L
F
B
D
W
C
VELOCITY SELECTOR

The static balance of the velocity selector was maintained to as high a degree as possible during all machining operations. This was done in order to reduce the amount of flexing the shaft must undergo during operation so as to minimize the occurrence of a shaft failure. All curved surfaces were maintained concentric to within ± 0.0001 in. with all horizontal surfaces maintained parallel within the same limit. In addition the four equally spaced threaded holes used to attach the cap C to the velocity selector were drilled and bored to the same geometry, and the threads rolled rather than tapped. This procedure does not remove any material (as does a cutting tap) and thus helps maintain balance. The bolts, B (Fig. 7), were constructed from 303 stainless steel with sixteen full 5/16-18 threads and drilled through their length to provide pump relief. The bolt heads were cut with a 3° retaining taper in order to maintain symmetry. Special sockets with matching 3° tapers were used for their installation and removal. The weight of all bolts was held to within ± 0.2 mg. With these precautions the static balance of the selector was highly preserved.

2. Molecular beam apparatus

The machine constructed to receive the velocity selector consists of three regions; the first two are

chambers in which beams are produced and collimated, the third is the chamber which houses the velocity selector and detector. In the view of the apparatus shown in Figure 8 the second beam chamber is not seen; it is located directly behind the velocity selector chamber perpendicular to the beam chamber shown. With the exception of pumps and baffles all the main components of the apparatus are constructed from stainless steel with heliarc welded joints. Each region is evacuated by its own diffusion pump; a manifold connecting the three chambers is provided for the evacuation of any chamber by pumps of any other. All gaskets used are teflon, neoprene, or silicone rubber O-rings. A collar, shock mounted from the frame, located under the top flange of the baffle chamber serves to support the machine. The frame is coupled to the floor by means of bonded rubber shock mounts, and a system of jack screws allows leveling of the instrument. Vibration elimination is further achieved by the use of bronze bellows in the lines connecting the diffusion pumps to their mechanical vacuum pumps. All other connections to the machine are made through small diameter (3/8 in. and less) soft copper tubing; this tubing is sufficiently flexible to require no additional vibration elimination.

The beam chambers are constructed from 6 in. diameter Ladish tees. Each is evacuated with its own 6 in. diameter

Fig. 8.-Cross-sectional view of two of the three main chambers of the apparatus (the second beam chamber being perpendicular to the one shown and located directly behind the velocity selector chamber).

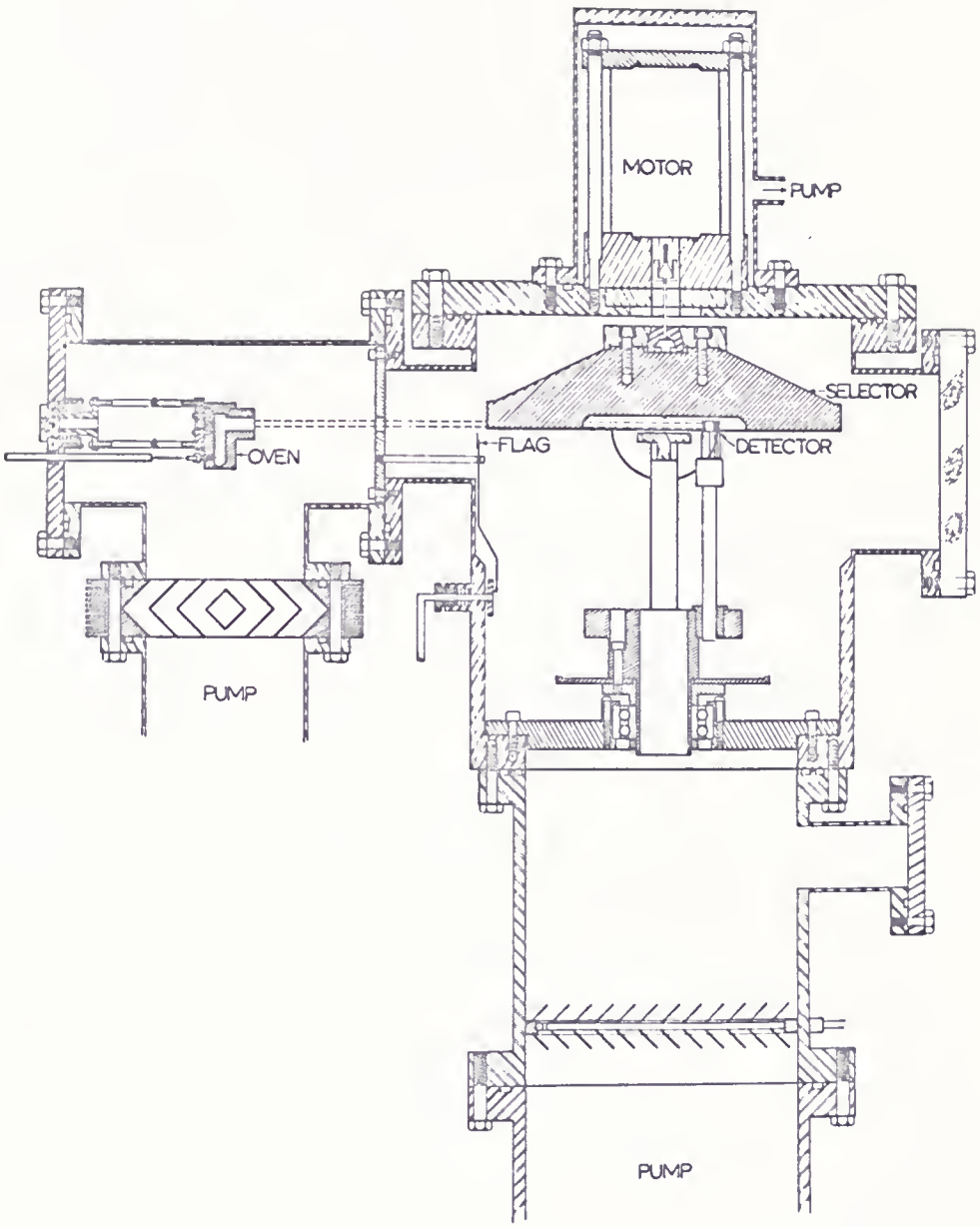
MOTOR
PUMP
SELECTOR
OVEN
FLAG
DETECTOR
PUMP
PUMP

oil diffusion pump backed by a 13 c.f.m. mechanical vacuum pump. Each has an air cooled circular chevron baffle[34] to retard the migration of oil from the diffusion pump into the high vacuum region. A Veeco RG-75 ionization gauge and a port that communicates with a McLeod gauge are provided in each chamber for the measurement of pressure.

The central chamber (Figure 8) of the apparatus contains, in addition to the velocity selector, the detector and mechanisms for the interruption of molecular beams (beam flags). Above this chamber is a smaller enclosure which contains the velocity selector drive motor. Both of these regions are evacuated by a CVC model MCF-1400 oil diffusion pump backed by a CVC E-70 mechanical vacuum pump. The velocity selector region is separated from the diffusion pump by a freon cooled chevron baffle. The line through which the motor chamber is evacuated communicates with the diffusion pump below the baffle; consequently, the gases given off from the motor are, to a great extent, not allowed to enter the velocity selector region. There are four main ports in the central chamber; two of these communicate with the beam chambers, the other two are 6.5 in. in diameter thus permitting ready accessibility to any portion of the chamber. The latter ports when fitted with lucite covers allow the operation of the velocity selector to be observed while the machine is under vacuum. Pressure

in the velocity selector region is monitored by a Veeco RG-75 ionization gauge and may be measured by a McLeod gauge. The two beam flags present in the chamber are so constructed that in their raised position the beams are interrupted. These flags are operated by independent mechanisms which convert rotary motion of a shaft through a Wilson seal in the chamber wall to linear motion of the flags. Bulkheads attached to the beam chamber ports, in addition to isolating the beam chambers, contain collimating slits which help define the molecular beam.

3. Beam formation

A cross-sectional view of the oven assembly used to generate a beam of alkali metal atoms is shown in Figure 9. This assembly is mounted on a flange which bolts onto the rear of a beam chamber. The oven is designed to accept glass ampules of alkali metal which are broken after the entire apparatus has been evacuated. It has rectangular geometry and is constructed from oxygen-free, high-conductivity copper. The opening in the top of the oven, through which the glass ampule is introduced, is sealed with a tapered plug, C, fabricated from the same material used for the oven. A modified 10-32 stainless steel allen cap screw, V, is provided to break the glass ampule which is located in the oven well. This screw is driven by means of an allen wrench attached to a 1/4 in. diameter shaft, S,

Fig. 9.-Oven assembly: A-alignment plug, B-double row ball bearing, C-oven cap, F-supporting flange, G-gear, H-holes to receive heaters, K-knees, L-lever, P-alignment port cap, R-ceramic ring, S-shaft, T-thermocouple location, V-ampule breaking screw, W-Wilson seal.

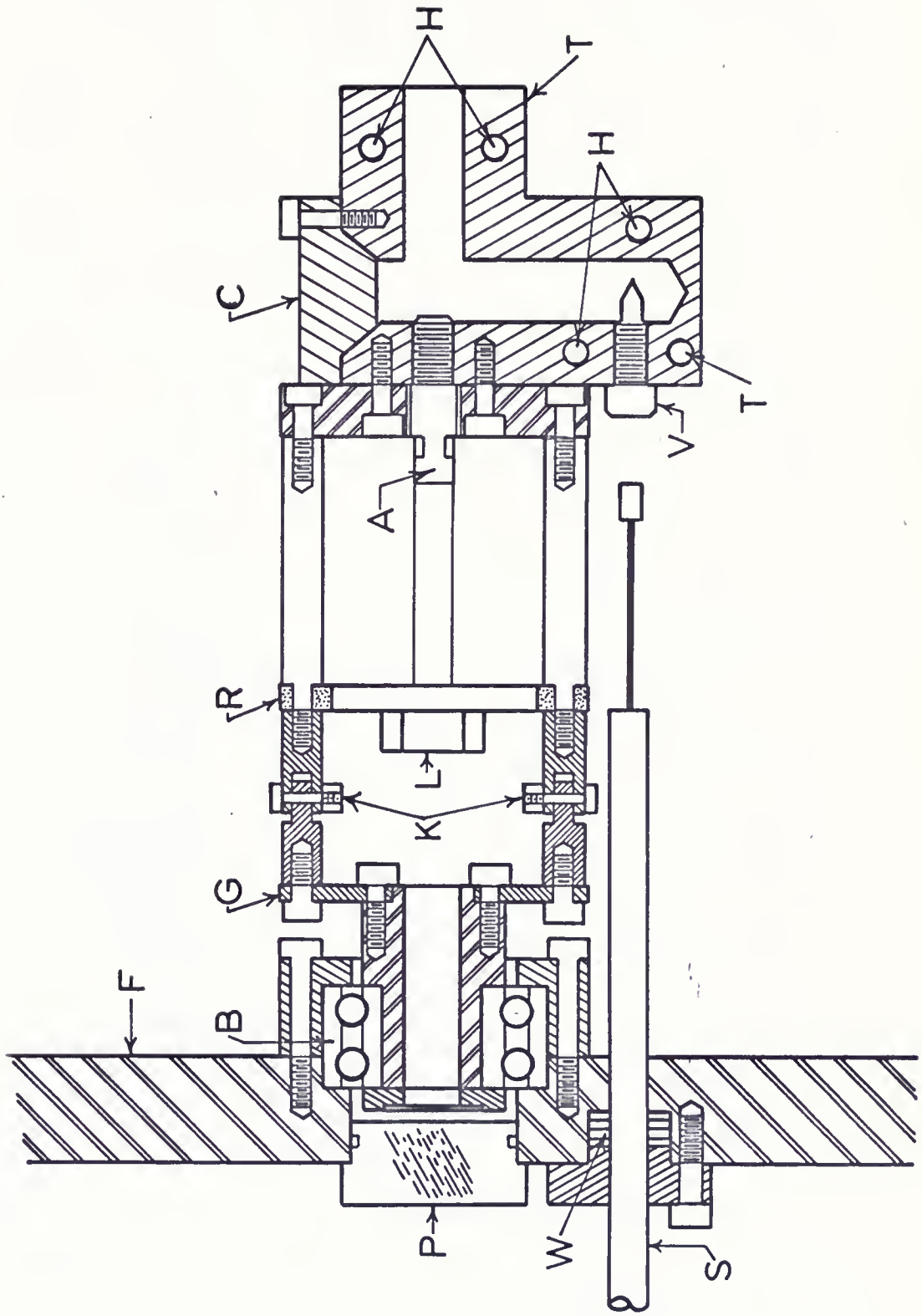
H
T
H
C
T
V
A
R
L
K
G
F
B
P
W
S

through a flexible wire; this shaft exits the vacuum system through a Wilson seal, W. Engagement of the allen wrench and screw V is assured during the ampule breaking operation by the following means. A portion of the shaft S outside the vacuum chamber is provided with 1/4 - 32 external threads; a fixture with internal matching threads is then screwed onto the shaft and attached securely to the compression cap of the Wilson seal after engagement of the allen wrench, thus fixing the position of the allen wrench with respect to the screw V. After the glass ampule is broken the fixture is released from the compression cap and used to jack the allen wrench away from the screw thus removing from the oven a possible heat sink. Razor blades[35] are used as slit jaws for the oven; their edges are maintained parallel by location of the blades with reference to the walls of a slot milled into the face of the oven. The width of the milled slot allows slit widths ranging from 0 to 0.020 in. to be used. The plug A is provided for optical alignment purposes; it is stainless steel and has 1/4 - 28 threads for insertion. Optical alignment of the oven is accomplished with the plug removed from the oven. Heat is supplied to the oven by means of four 1/8 in. diameter tubular heaters[36] located in holes H. These heaters are arranged and powered so as to maintain the slit region at a slightly higher temperature than the rest of the

oven. The temperature of the oven is monitored by two iron-constantan thermocouples located at positions T.

By virtue of its mount, the oven has two degrees of freedom; these are: rotation about the beam axis and movement perpendicular to the plane of the beam (pivoting). Both of these actions are controlled from outside the vacuum chamber. The entire oven assembly is supported by the inner race of the double row ball bearing B (Figure 9), the outer race of the bearing being securely affixed to the supporting flange. Rotation is achieved by the action of a spur gear on the oven mount gear G. The spur gear is attached to a 1/4 in. diameter shaft which extends through the supporting flange by means of a Wilson seal. The oven is supported on four stainless steel tubular stilts mounted on a ceramic ring, R (Figures 9 and 10). Between the ring and gear G are located two knees, K, which enable the oven to be pivoted. Pivoting is produced by the action of a shaft (entering the vacuum system through a Wilson seal) on a lever L attached to the ceramic ring (Figures 9 and 10). This shaft is threaded through a support affixed to the flange, and the lever is held against it by means of a tension spring.

A liquid nitrogen cooled shield (Figure 10) is located directly in front of the oven. Practically all the alkali metal effusing from the oven that does not constitute

Fig. 10.-Photograph of the oven and scattering chamber assembly with the liquid nitrogen trap and cold shield in place.

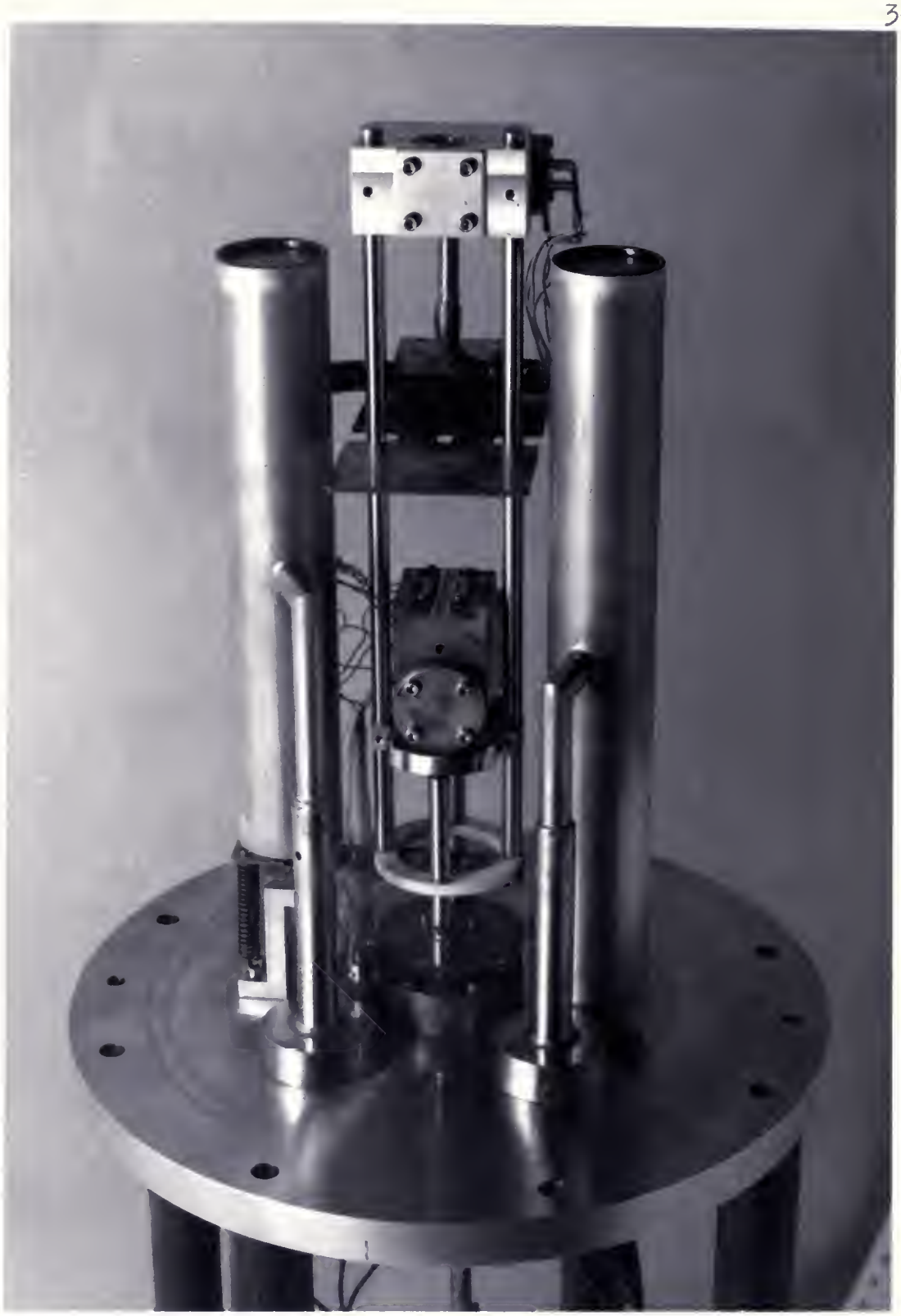

the beam is removed by condensation on the shield. In addition the shield reduces the background pressure by means of cryogenic pumping.

4. Scattering chamber

Experiments conducted thus far have involved the use of one beam with a scattering chamber located between the beam oven and the velocity selector. These experiments have been conducted in order to obtain data to which the results of future double beam experiments may be compared.

The scattering chamber is mounted directly to the oven assembly (Figure 10). Two of the four stilts that support the oven are replaced by 1/4 in. diameter precision shafting. These shafts are attached to the ceramic ring of the oven assembly and located by means of reamed holes in the plate supporting the oven; they pass along the side of the oven and extend beyond it. Two 1/4 in. diameter reamed holes, H (Figure 11), in the scattering chamber are precisely located so as to accept these shafts and align the scattering chamber with the oven.

The scattering chamber is constructed of aluminum. A well is provided (Figure 11) to accept a modified RCA model 1946 thermocouple gauge (Appendix I). This gauge is constructed using only the wires from the RCA tube. These wires are attached to a support system that enables them to be introduced into the 1/2 in. diameter well. An iron-

Fig. 11.-Diagram of the scattering chamber: S-body of chamber, TCG-thermocouple gauge, G-teflon gaskets, P-plugs with 0.004 x 1/4 in. slits, L-blank off cap.

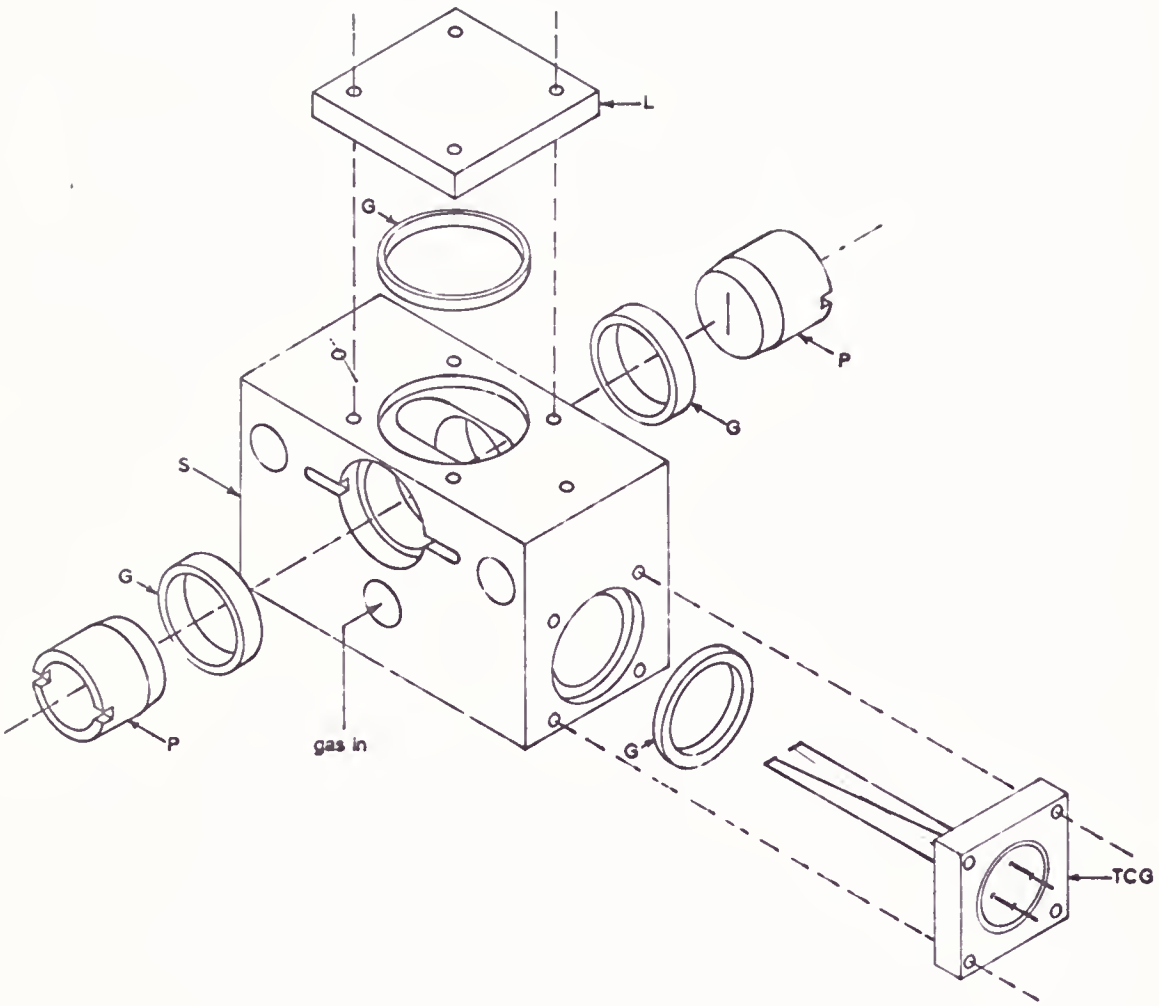
L
G
P
G
S
G
P
gas in
G
TCG

constantan thermocouple is attached to the support flange of the gauge to allow monitoring of the scattering chamber temperature. A port which communicates with the thermocouple well is provided for introduction of the scattering gas through a 1/4 in. copper tube extending to the outside of the vacuum system. The scattering path length is determined by plugs inserted into a 1/2 in. diameter reamed hole whose axis corresponds to the central beam axis (when the chamber is on its mount). The plugs have a wall thickness of 0.002 in. at their ends; they are provided with 0.004 x 1/4 in. slits cut by a 0.004 in. slotting saw. Teflon rings with inner diameters slightly less than 1/2 in. are placed in steps at either end of the 1/2 in. hole; it is these rings which effect a seal about the plugs and cause them to remain in position. Each plug's open end is slotted so that the position of its slits may be precisely located by the alignment of these slots with corresponding ones milled into the body of the scattering chamber. The region between the plugs communicates with the thermocouple well by means of a 1/4 in. milled slot. The distance between the ends of the plugs is 0.001 in. $\pm$ 0.0005 in.

For calibration purposes the plugs in the scattering chamber are replaced by a 0.498 in. diameter shaft which passes through both teflon rings and is held in place by compression caps. This arrangement seals the chamber and

in addition serves to extrude the teflon rings so they maintain their ability to position the plugs.

5. Detector

The beam of alkali atoms is detected on a tungsten surface ionization (Langmuir-Taylor) detector.[37,38] The alkali metal atom striking the hot tungsten surface is adsorbed; it may then give up an electron and evaporate as a positive ion. All experiments thus far have involved the use of cesium beams; the ionization efficiency for cesium on a tungsten surface at 1300°K or higher is 1.00.[39]

The detector is mounted from a spiroid gear whose axis of rotation coincides with that of the velocity selector. This allows the detector to be moved about the scattering zone. The spiroid gear is driven from outside the vacuum system through a modified Wilson seal. A full rotation of the selector drive shaft produces movement of the detector through 1 deg. of arc.

A schematic diagram of the detector is shown in Figure 12. Beam atoms reach the hot tungsten filament D by passing through slits in electrodes C and G. The 0.003 in. diameter tungsten filament[40] is spot welded at the top to a 0.040 in. diameter support rod and at the bottom to a 0.010 in. diameter tungsten spring, which in turn is spot welded to the lower support. Power to heat the filament is

Fig. 12.-Schematic diagram of detector: D-heated tungsten filament, P-repeller, G-guard electrode, F1 and F2-focusing electrodes, C-collector electrode.

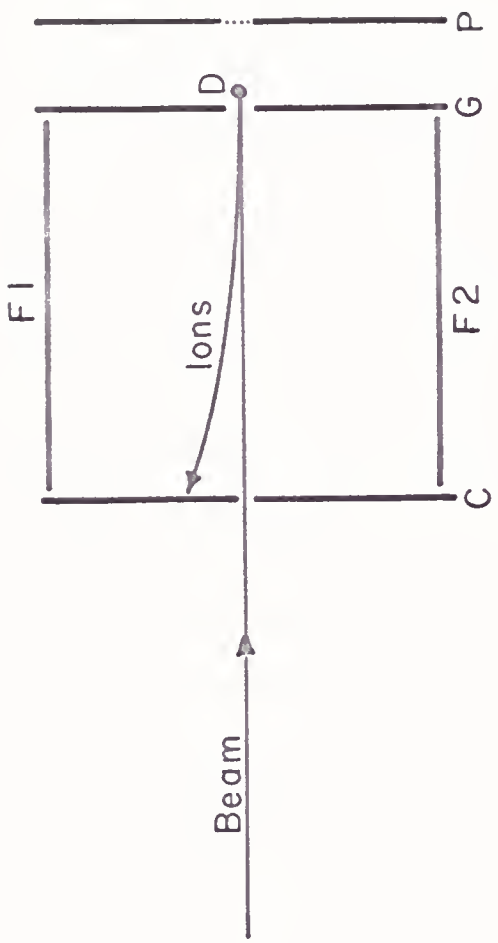
P
D
G
F1
Ions
F2
C
Beam

supplied by a 6 volt lead storage battery. The filament and repeller P are at a positive potential with respect to ground with the repeller being at a slightly higher potential than the filament. The repeller has a grid covered window to allow optical alignment. The guard electrode G has a slit 3/8 in. long and .063 in. wide; it is employed to collect all ions from those parts of the filament not exposed to the beam. The potential on G is negative with respect to the filament. Those positive ions resulting from beam atoms striking the filament are accelerated through the slit in G and focused by F1 and F2 to strike to the right or left of the 0.010 in. slit in the collector electrode C (located at ground). These ions striking C are read as a current with the aid of a Cary model 31 vibrating reed electrometer. All potentials to the electrodes and filament are furnished by lead storage batteries, with the repeller being ~ 48 volts off ground.

B. Procedure

The procedure for the investigation of transmission characteristics of the velocity selector and the measurement of cross-sections will be outlined.

1. Measurement of transmission characteristics of the velocity selector

The positions of the oven, scattering chamber, and

detector are determined by the location of the velocity selector within the apparatus; consequently, the alignment of the apparatus must be checked. Provision is made for the accurate location of the motor (from which the selector is suspended) in regard to the top flange of the selector chamber (Figure 8). This provision and the ability to level the apparatus, thus placing the motor shaft in a vertical position, enable the velocity selector's position with respect to the apparatus to be reproducible. During the introduction of the velocity selector into the machine the flexible shaft (Figure 7) is sometimes bent slightly. The condition of the shaft is determined (after leveling the machine) by viewing the lower edge of the selector telescopically through the front port of the apparatus. If the shaft is bent, the lower edge will rise and fall as the selector is turned slowly. This occurrence is corrected by lifting the rim of the selector gently by hand at its low point, the test being repeated until the flat surface of the rotor is horizontal. After the selector has been positioned in this manner the alignment of the oven, scattering chamber, and detector with the selector is checked optically. Checks such as described above have never revealed any deviations from the initial alignment of the apparatus.

The measurement of transmission characteristics does not necessitate the use of a scattering chamber; consequently, this component along with the cold shield (Figure 10) were not present in the apparatus. The slit located in the bulkhead separating the beam chamber from the velocity selector chamber was set at 0.020 in. and used to collimate the beam. A shield was provided just below the inner rim of the velocity selector to mask out all beam particles that did not traverse the entire selector. The experimental constants are listed in Table 1. With these modifications accomplished, the transmission characteristics of the selector were determined.

After the alignment of the apparatus is checked, a glass ampule of cesium is introduced into the oven and the assembly placed in the beam chamber. The apparatus is then initially evacuated by a small mechanical vacuum pump. After the initial pump down, the machine must be re-leveled to compensate for the external atmospheric pressure exerted on evacuated bellows in the fore line. The diffusion pumps then reduce the pressure to operating conditions (3×10^{-6} mm Hg for the beam chamber, and 1×10^{-6} mm Hg for the velocity selector chamber). Under vacuum the oven is outgassed by heating to a temperature approximately 20°C above that at which it will be operated, and the filament aged at 0.7 amp. for several hours.

Table 1.--Operating Conditions for Measurement of Transmission of a Maxwellian Beam of Cesium Atoms.

Oven slit width	0.004 in.
Collimating slit width	0.020 in.
Detector width (tungsten wire)	0.003 in.
Beam height	2.5 in.
Length of beam path in collimating chamber, ℓ_1	4.00 in.
Length of beam path in scattering chamber, ℓ_2	12.375 in.
Oven temperature	405°K
Pressure in beam chamber	1×10^{-6} Torr.
Pressure in velocity selector chamber	8×10^{-7} Torr.
Radial position of detector, R_d	1.875 in.

Approximately two hours before the measurements are to begin the oven is turned on and allowed to reach operating temperature (130°C). At 130°C and with 0.004 in. wide oven slits the mean free path of the Cs in the oven is approximately three times the slit width. During the warm up time, the velocity selector is accelerated to operating speed. The selector motor is driven by a variable frequency two phase electronic power supply through two ganged 8 amp. variacs. During acceleration the rotor passes through regions of relative instability before the shaft is flexed sufficiently to permit the selector to spin about its true inertial center. The speed of the velocity selector is determined stroboscopically; the output of the stroboscope being registered on an electronic counter whose count period is determined by another counter monitoring the 60 cps line frequency. Also, during the oven warm up period, the detector wire is flashed for 1 min. at 1 amp.; this cleans the filament and reduces the background.

After the oven is stabilized at the desired temperature, it and the detector are positioned to allow maximum transmission at the selector speed for which this condition applies when the detector is in the beam axis (Section III, A). With the oven and detector properly aligned, measurements are ready to be made.

The selector is accelerated to the highest speed for which measurements are to be made. A beam profile is scanned at this speed by moving the detector completely through the beam while indicating every 1/4 deg. of arc. These and following measurements are made using the electrometer (in the current sensitive mode) whose output is recorded on the chart of a Leeds and Northrup Speedomax H recorder. The velocity selector motor is then decoupled from its power supply and the rotor allowed to coast. Alternately the transmitted intensity and the background (beam interrupted by flag) are measured. During each of these periods the oven temperature and selector speed (at a particular time) are determined. The oven temperature is determined by reading the emf generated by the iron-constantan thermocouple attached to the oven with a Leeds and Northrup type K-2 potentiometer. The speed of the selector is determined stroboscopically by setting the stroboscope to a speed slightly below that of the selector and then waiting for the stroboscopic image to stabilize (stroboscope and selector synchronized) at which moment a timing mark is placed on the recorder chart. Therefore, the speed of the selector at the time of the mark was made is that for which the stroboscope is then set; the output of the stroboscope is then determined by the electronic counting method described above and recorded. Since the time between successive

measurements is short, a linear interpolation between adjacent measured intensities is acceptable; thus the transmitted intensity is proportional to the distance between the interpolated intensity at a particular selector speed and the background trace on the chart. During the course of these measurements the amplification factor of the electrometer is changed; consequently it is necessary to normalize all the data to conform to a particular amplification factor (in this case the 300 mv scale of the electrometer). The above procedure was followed for velocity selector speeds from 8000-1800 RPM.

2. Measurement of total cross-sections

All components described in the first section of chapter are present in the apparatus. The mask described previously is removed from under the velocity selector and placed across the bulkhead slit at a height which corresponds to the bottom of the selector. The electrometer used to amplify the detector signal is operated in the rate of change mode with the beam intensity being proportional to the slope of the recorder trace. Modifications made to the recorder enable it to trip three switches as the pen moves up scale. The first and third switches are set at a precise distance (3.000 in.) apart and used to start and stop an electronic counter. This counter receives a 1000 cycle signal from a low frequency oscillator.

Thus, the precise time the recorder pen takes to move a specific distance is obtained. The ratio of the counter reading to the distance the recorder pen moves is proportional to the slope of the recorder trace and hence the beam intensity. The second switch actuated by the recorder is located midway between the first and third; it places a small blip on the recorder chart indicating the position at which the slope of the trace is taken. The other two switches also place blips on the recorder chart to indicate initiation and termination of the timing operation. A fourth blip is placed on the recorder chart by a switch located directly in front of the apparatus; this blip is used to mark the point at which the selector speed is determined. All mechanisms that place blips on the recorder chart also cause a time recorder to print out the time to the nearest 0.01 sec.

Before cross-sections measurements can be made, the thermocouple gauge in the scattering chamber must be calibrated. The calibration plug is inserted in scattering chamber, and this chamber along with the oven is placed in the beam chamber. The entire apparatus is pumped down to simulate operating conditions. Power is supplied to the heater of the gauge by means of the 2 volt storage battery. The current drawn by the heater is held to approximately 59 ma. by inclusion of appropriate fixed resistors. The

gauge heater is operated for at least half a day to allow time for it to stabilize. The oven is heated to operating temperature and liquid nitrogen added to the trap; this allows the temperature of the scattering chamber to stabilize at approximately 50°C (for an oven temperature of 160°C). Calibration of the gauge may now begin. With the gauge under high vacuum (pumped on by the other beam chamber's diffusion pump) a reading of its output E_o, is made with the K-2 potentiometer. Pumping on the gauge is then terminated, and gas is introduced into the scattering chamber through a leak valve with a 1000:1 taper until the desired pressure is obtained, at which time the flow of gas is interrupted (pressure is prevented from building on the low pressure side of leak valve by engaging an oil diffusion pump located in the gas handling system associated with the machine). After the pressure in the system has equilibrated, a portion of the gas is trapped in the McLeod gauge and the thermocouple gauge output, E, is read. The thermocouple gauge is pumped down and three successive readings of the former pressure are made on the trapped gas in the McLeod gauge (which is read with a cathatometer). While the McLeod gauge is being read, E_o is again determined. The temperature of the McLeod gauge region and that of the scattering chamber is also recorded. This procedure is followed over the pressure range 0.5 to 5.0 microns in 0.5 micron increments.

After calibration of the thermocouple has been accomplished the machine is vented with dry nitrogen and the oven and scattering chamber removed. It should be noted at this point that, as stated previously, the alignment of the machine has never been observed to be affected by removal of either the oven assembly or velocity selector from the machine; consequently, the alignment checking procedure is no longer repeated after removal of either of these components. The oven is loaded with a glass ampule of Cs and replaced in the machine. The same procedure (prior to actual measurements) as outlined previously is now followed, the one exception being that liquid nitrogen is added to the trap in the beam chamber before the Cs ampule is broken. Once liquid nitrogen has been added it is important that the trap never be allowed to become empty during a run; this requires refilling the trap at least every half hour.

Prior to the actual taking of data the pressure in the scattering chamber must be adjusted (by means of the above mentioned leak valve) to produce a beam attenuation of about 20 per cent at the highest selector speeds (8000 RPM). This operation must, of course, be carried out at constant velocity selector speed. Having established the appropriate pressure in the scattering chamber, measurements may now be taken.

The beam flag is raised to interrupt the beam and the background is measured. An amplification factor for the electrometer (in the rate of change mode) is chosen such that the slope of the recorder trace is not more than 1.5. The velocity selector is decoupled from its power supply and allowed to decelerate. Alternately the unscattered beam intensity I_0 (gas out of scattering chamber) and scattered beam intensity I (gas in) are measured. These measurements are obtained in the manner previously described for the electrometer in the rate of change mode. During the time I_0 is being traced by the recorder the output, E_o, of the thermocouple gauge and the temperature of the oven are read on the potentiometer. Between the measurement of I_0 and I the speed of the selector at a particular time is determined; the procedure used is the same as has been described for the transmission characteristic determination. After sufficient time has elapsed for the equilibration of gas in the scattering chamber, I is determined; at the same time E for the thermocouple gauge and the temperature of the scattering chamber are read with the potentiometer. This procedure is followed until the selector has reached a speed of 1000 RPM (usually in 14 or 15 hours). Typical operation conditions under which these measurements are taken are listed in Table 2.

Table 2.--Typical Operation Conditions for Measurement of Cross-Sections of Cesium with Nitrogen and Argon.

Oven slit width	0.002 in.
Scattering chamber slit width	0.004 in.
Scattering chamber length	0.100 in.
Detector width (tungsten wire)	0.003 in.
Beam height	0.250 in.
Distance between oven and scattering chamber	4.95 in.
Distance between scattering chamber and velocity selector	12.00 in.
Pressure in beam chamber (gas out of scattering chamber)	6×10^{-7} Torr.
Pressure in beam chamber (gas in scattering chamber)	9×10^{-7} Torr.
Pressure in velocity selector chamber	2.0×10^{-6} Torr.
Radical position of detector	1.875 in.
Angular resolving power	3 min.

The time interval between successive measurements is short allowing linear interpolations to be made between successive I_0's and I's; in addition this type of interpolation may be used for the determination of selector speeds between timing marks. Consequently, it is possible to obtain two cross-section measurements from the determination of one pair of intensities; these measurements are made at the selector speed corresponding to the time at which the slope of the particular trace (I or I_0) is measured. It is from the scattering chamber pressure and the ratio of I_0/I (at a particular velocity selector speed) that the cross-sections are calculated.

III. THEORY

A. Transmission Characteristics of a Parallel Wall, Spiral Groove Velocity Selector[41]

Parameters of the velocity selector are given in Table 3. All graphical representations of this section are for the specific geometry of this selector. The coordinate system to be used in this analysis is shown in Figure 13. The projected trajectory of a point moving with velocity v_M corresponds to the center line of a groove when the selector rotates with an angular speed of ω; this trajectory is defined by the polar angle θ and the radial distance r from the center of the selector. The equation of the center line of a groove is

$$\theta_M = (\omega/v_M)\,(R_1 - r) = (\theta_0/\ell)\,(R_1 - r)\,, \qquad (1)$$

where the substitution $\omega/v_M = \theta_0/\ell$ has been used. Equation (1) is obtained by equating $(R_1 - r)/v_M$, the time required to move a radial distance $R_1 - r$, to θ/ω, the time for rotation of the selector through the angle θ. The equations for the walls of the groove are obtained in like manner with the exception that provisions must be made for the walls to remain parallel to the center line; the quantity $\sin^{-1}(a/r)$ accomplishes this purpose, and the equations are

Table 3.--Velocity Selector Parameters.

R_1	6.500 in.
R_2	3.000 in.
ℓ	3.500 in.
θ_0	0.1297 rad.
a	0.0345 in.
Groove depth	0.250 in.
Number of grooves, n	148
$T_{r,min}(\gamma = 0)$	0.319
$T_{r,max}(\gamma = 0)$	0.681
Resolution	17.3%

Fig. 13.-Coordinate system for velocity selecting grooves.

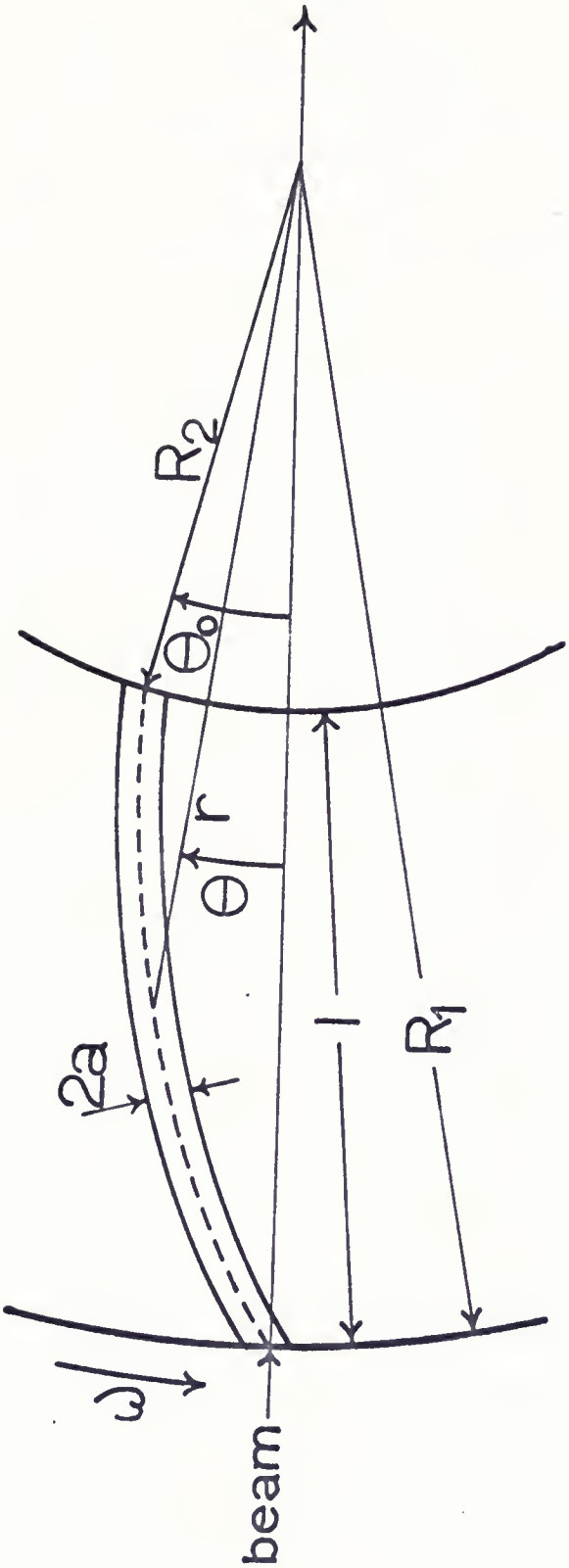
R2
θo
r
θ
2a
l
R1
ω
beam

$$\text{Upper wall:}\quad \theta_U = (\theta_o/\ell)(\sqrt{R_1^2-a^2} - \sqrt{r^2-a^2}) + \sin^{-1}(a/r)$$

$$\text{Lower wall:}\quad \theta_L = (\theta_o/\ell)(\sqrt{R_1^2-a^2} - \sqrt{r^2-a^2}) - \sin^{-1}(a/r) \qquad (2)$$

Several approximations may be made to simplify Eqn. (2). For $r \gg R_2$ (which is always the case during selection) the groove width, a, is much less than r; consequently the small angle approximation for the sine function can be used. In addition the quantities $(R_1^2-a^2)^{1/2}$ and $(r^2-a^2)^{1/2}$ may be approximated by R_1 and r, respectively. Upon introducing these approximations and requiring $\theta_L(R_1) = 0$ when $t = 0$, Eqns. (1) and (2) become

$$\begin{aligned} \theta_M &= (\theta_o/\ell)(R_1-r) + a/R_1 + \omega t \\ \theta_U &= \theta_M + a/r \\ \theta_L &= \theta_M - a/r \end{aligned} \qquad (3)$$

The outer limit of the groove substends an angle $2a/R_1$ from the center of the selector. Therefore, the time interval during which a narrow beam of molecules, incident normal to the selector, can enter the groove is $0 < t < -2a/R_1\omega$. If a reduced time $t_r = R_1\omega t/2a$ is defined, the admittance interval becomes $0 < t_r < 1$. Molecules with velocity v entering the selector during this time interval will have projected trajectories given by

$$\theta = (\omega/v)(R_1-r) = (R_1-r)/(R_1V_r) \quad , \qquad (4)$$

where a reduced velocity $V_r = v/\omega R_1$ has been defined.

At time t_r only those molecules which enter the groove with reduced velocities in the range $V_r(t_{r,max}) < V_r < V_r(t_{r,min})$ will be transmitted. Those molecules with velocities outside this range will undergo collisions with the groove wall and be taken out of the beam. The positions at which these beam molecules strike the wall are given by

$$r_U = (R_1/2L_V)\left\{L_V + a(2t_r-1) \pm [(L_V + 2at_r-a)^2 - 4aL_V]^{1/2}\right\} \qquad (5)$$

$$r_L = (R_1/2L_V)\left\{L_V + a(2t_r-1) \pm [(L_V + 2at_r-a)^2 + 4aL_V]^{1/2}\right\} \qquad (6)$$

where

$$L_V = R_1^2\,\omega\,(1/v-1/v_M) = R_1/V_r - R_1^2\theta_o/\ell \ . \qquad (7)$$

Those molecules for which $V_r < V_r(t_{r,min})$ will strike the upper wall. Equations (5) and (6) are obtained by solving Eqns. (4) with (2). Beam molecules that are transmitted by the selector follow one of two types of trajectories. The first or oblique trajectory, is one which moves continuously toward, or away from, a wall of the groove; the second or tangential trajectory, exhibits what may be called a turning point in that it moves first toward a groove wall and then away from it. It is this latter type which usually determines the velocity range transmitted by the groove. Molecules entering the groove at

time t_r with velocity V_r will be transmitted provided Eqns. (5) and (6) have no real roots in the range $R_1 \gg r \gg R_2$. Those paths for which there exist double roots in this range will make grazing collisions with one of the groove walls thereby determining the maximum and minimum transmitted reduced velocities. It is for these latter cases that the discriminants of Eqns. (5) and (6) are zero. Therefore, the limiting L_V's may be obtained as

$$L_{V,min,tan} = a\left\{1+[2(1-t_r)]^{1/2}\right\}^2 \qquad R_1 \gg r_{U,tan} \gg R_2 \qquad (8)$$

$$L_{V,max,tan} = -a[1+ (2t_r)^{1/2}]^2 \qquad R_1 \gg r_{L,tan} \gg R_2 \qquad (9)$$

where

$$r_{U,tan} = R_1/\left\{ 1 +[2(1-t_r)]^{1/2}\right\} \qquad (10)$$

$$r_{L,tan} = R_1/[1 + (2t_r)^{1/2}] \quad . \qquad (11)$$

The trajectories will be tangential for $r_{U,tan}$ or $r_{L,tan} > R_2$. In most cases $r_{U,tan}$ or $r_{L,tan}$ become less than R_2 during the interval $0 \ll t_r \ll 1$ so that a transition occurs between tangential and oblique trajectories; consequently some velocities are limited by collisions at the inner edge of the groove walls. The time T_r at which the transition occurs is found by setting Eqns. (10) and (11) equal to R_2,

$$T_{r,max} = 1 - T_{r,min} = \ell^2/2R_2^2 \quad . \qquad (12)$$

In order to arrive at the oblique limited velocities the limiting L_V's must first be obtained. This is accomplished by setting r_U and r_L (Eqns. (5) and (6)) equal to R_2,

$$L_{V,min,ob} = (R_1\ a/\ell)[(R_1+R_2)/R_2-2t_r] \qquad t_r < T_{r,min} \qquad (13)$$

$$L_{V,max,ob} = -(R_1\ a/\ell)(\ /R_2+2t_r) \quad . \qquad t_r > T_{r,max} \qquad (14)$$

The limiting oblique reduced velocities are obtained by equating Eqns. (13) and (14) to (6) and the limiting tangential reduced velocities by equating Eqns. (8) and (9) to (6); so that there results

$$V_{r,min,ob} = \ell[R_1\theta_o+a(R_1+R_2)/R_2-2at_r]^{-1} \qquad 0 \leqslant t_r \leqslant T_{r,min} \qquad (15)$$

$$V_{r,min,tan} = \ell\{R_1\theta_o + (a\ell/R_1)[1 + (2-2t_r)^{1/2}]^2\}^{-1} \qquad T_{r,min} \leqslant t_r \leqslant 1 \qquad (16)$$

$$V_{r,max,tan} = \ell\{R_1\theta_o - (a\ell/R_1)[1 + (2t_r)^{1/2}]^2\}^{-1} \qquad 0 \leqslant t_r \leqslant T_{r,max} \qquad (17)$$

$$V_{r,max,ob} = \ell(R_1\theta_o - a\ell/R_2 - 2at_r)^{-1} \quad . \qquad T_{r,max} \leqslant t_r \leqslant 1 \qquad (18)$$

Figure 14 shows a shaded area on the V_r, t_r plane which represents the transmissions of the present selector. There exist slight discontinuities at $t_r = T_{r,min}$ and $T_{r,max}$; however, the scale of the plot is such as to render these

Fig. 14.-Plot of transmitted reduced velocities versus reduced time of arrival at edge of velocity selector.

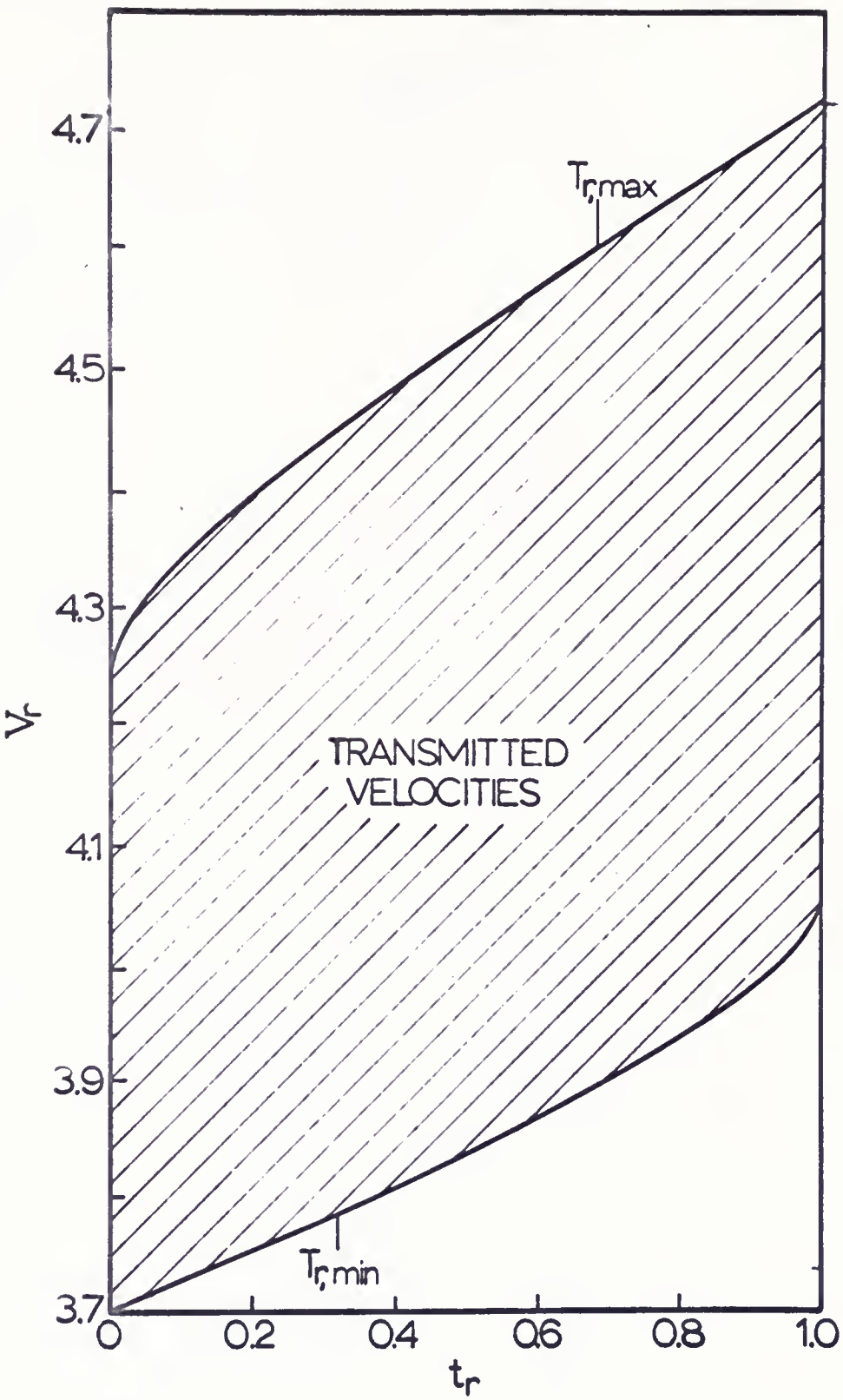
4.7
4.5
4.3
4.1
3.9
3.7
V_r
$T_{r,max}$
TRANSMITTED
VELOCITIES
$T_{r,min}$
0
0.2
0.4
0.6
0.8
1.0
t_r

discontinuities non-evident. The length of time a groove will be capable of transmitting molecules with a particular reduced velocity, V_r, is found from the length of the horizontal line through V_r that spans the shaded area. As can be seen, the groove is completely transparent to reduced velocities in the range 4.08 to 4.24. The fraction of total time $f(V_r)$ a groove will transmit a particular reduced velocity can be obtained by solving Eqns. (15) - (18) for t_r; thus

$$f_t(V_r) = t_r = R_1\theta_o/2a - (R_1-R_2)/2R_2 - \ell/2aV_r \qquad V_1 \leqslant V_r \leqslant V_2 \qquad (19)$$

$$f_t(V_r) = t_r = (1/2)[1 - (R_1/a)(1/V_r - R_1\theta_o/\ell\ )] + [(R_1/a)(1/V_r - R_1\theta_o/\ell\ )]^{1/2} \qquad V_2 \leqslant V_r \leqslant V_3 \qquad (20)$$

$$f_t(V_r) = 1 \qquad V_3 \leqslant V_r \leqslant V_4 \qquad (21)$$

$$f_t(V_r) = 1 - t_r = (1/2)[1 + (R_1/a)(1/V_r - R_1\theta_o/\ell\ )] + [(R_1/a)(R_1\theta_o/\ell - 1/V_r)]^{1/2} \qquad V_4 \leqslant V_r \leqslant V_5 \qquad (22)$$

$$f_t(V_r) = (1 - t_r) = -R_1\theta_o/2a + (R_1+R_2)/2R_2 + \ell/2aV_r. \qquad V_5 \leqslant V_r \leqslant V_6 \qquad (23)$$

If the above equations are plotted (Figure 15) a characteristic transmission profile is obtained for the particular selector. The reduced velocity distribution function for a transmitted pulse is

$$F(V_r)dV_r = f_t(V_r)I(V_r)dV_r \quad , \tag{24}$$

where $I(V_r)$ is the reduced velocity distribution function in the beam before velocity selection takes place. The transmitted intensity of a single pulse can be obtained, if $I(V_r)$ is known, by

$$i_\omega = \int_{V_1}^{V_6} f_t(V_r)I(V_r)dV_r \quad . \tag{25}$$

The total transmitted intensity then is made up from contributions of all pulses and is given by

$$I_\omega = i_\omega \, n\omega/2\pi \quad , \tag{26}$$

where n is the number of grooves in the selector and ω is the angular speed of the selector in rad./sec.

In order to glean as much information as possible from scattering experiments performed using this type of velocity selector, it is necessary to know the intensity and velocity distribution at the scattering zone (r = 0) as a function of time. This may be accomplished by considering a molecule with velocity v arriving at the outer edge of the selector at time t; the time of arrival at the

Fig. 15.-Characteristic transmission profile showing fractional reduced time f_t that a groove will transmit molecules arriving at the selector with normal incidence.

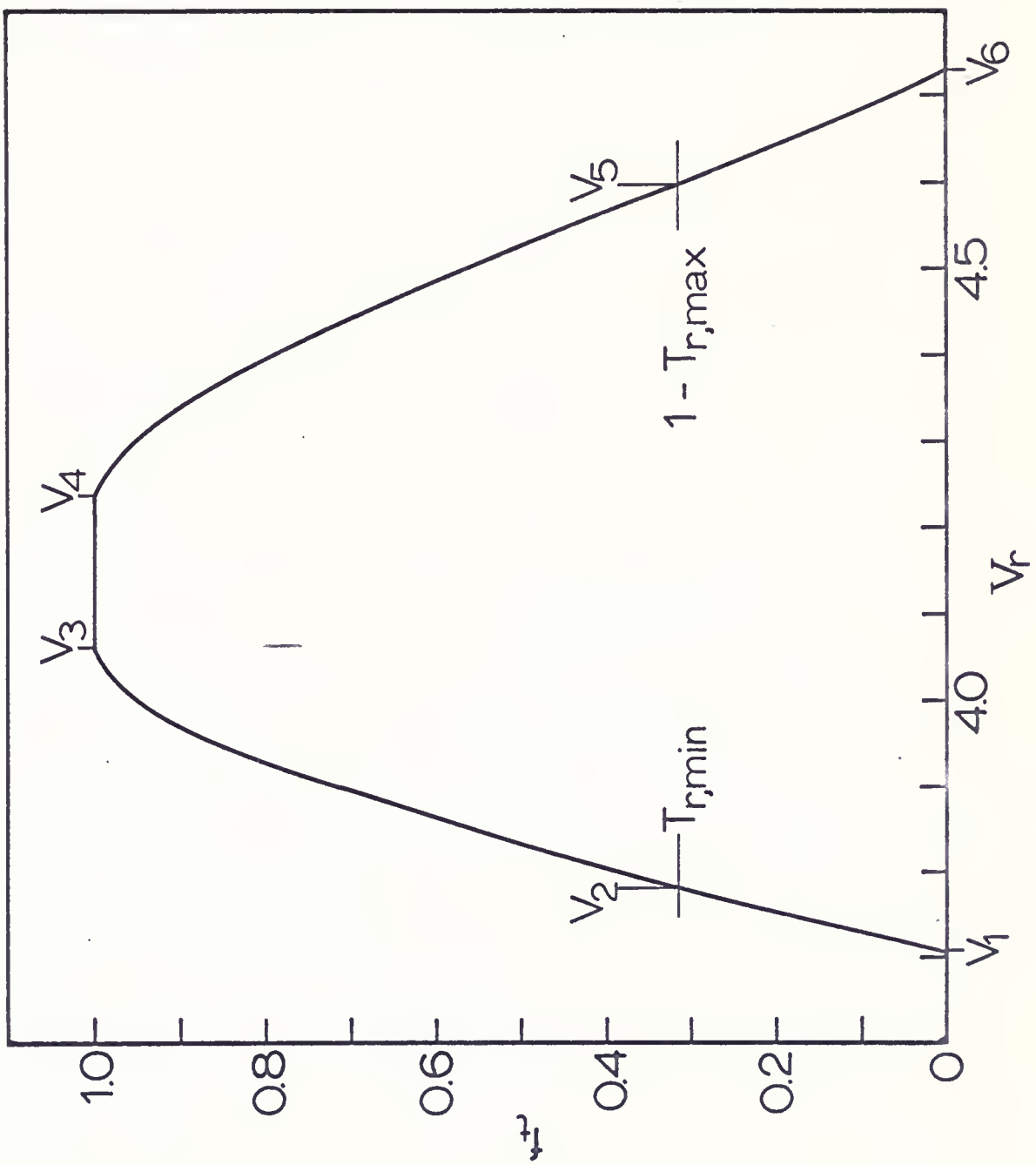
1.0
0.8
0.6
0.4
0.2
0
T_r
V_1
V_2
V_3
V_4
V_5
V_6
$T_{r,min}$
$1 - T_{r,max}$
4.0
4.5
V_r

scattering zone is $t + R_1/\omega$ (and in terms of reduced variables, $t_r - R_1/2aV_r$). The transformation $t_r \rightarrow t_r - R_1/2aV_r$ acting on the reduced velocities to be transmitted taken as a function of the reduced time of arrival at the edge of the selector generates the reduced velocity distribution function in terms of the reduced time of arrival at the scattering zone. This transformation is illustrated in Figure 16. A vertical line between ABC and ADC and through t_r indicates the range of reduced velocities arriving at the scattering zone at time t_r. The locus of points described by AB and CD are hyperbolas given by

$$\text{AB:} \quad V_r = R_1/2at_r \tag{27}$$

$$\text{CD:} \quad V_r = R_1/2a(1 - t_r) \quad . \tag{28}$$

The sides BC and DA are obtained by substitution of $t_r = t_r - R_1/2aV_r$ into Eqns. (15) - (18). The velocity spread, ΔV_r, at the scattering zone as a function of reduced time is shown in Figure 17. Dashed lines indicate discreet pulses; as can be seen for the present selector there is an overlap of transmitted pulses at the scattering center. This overlap creates a ripple superimposed on a constant transmitted intensity. At the scattering zone the resultant time dependent intensity is indicated by the solid line. That portion of the transmitted pulse indicated in Figure 17 by AB is determined entirely by the velocity distribution

Fig. 16.-Time dependent distribution of transmitted velocities at scattering zone.

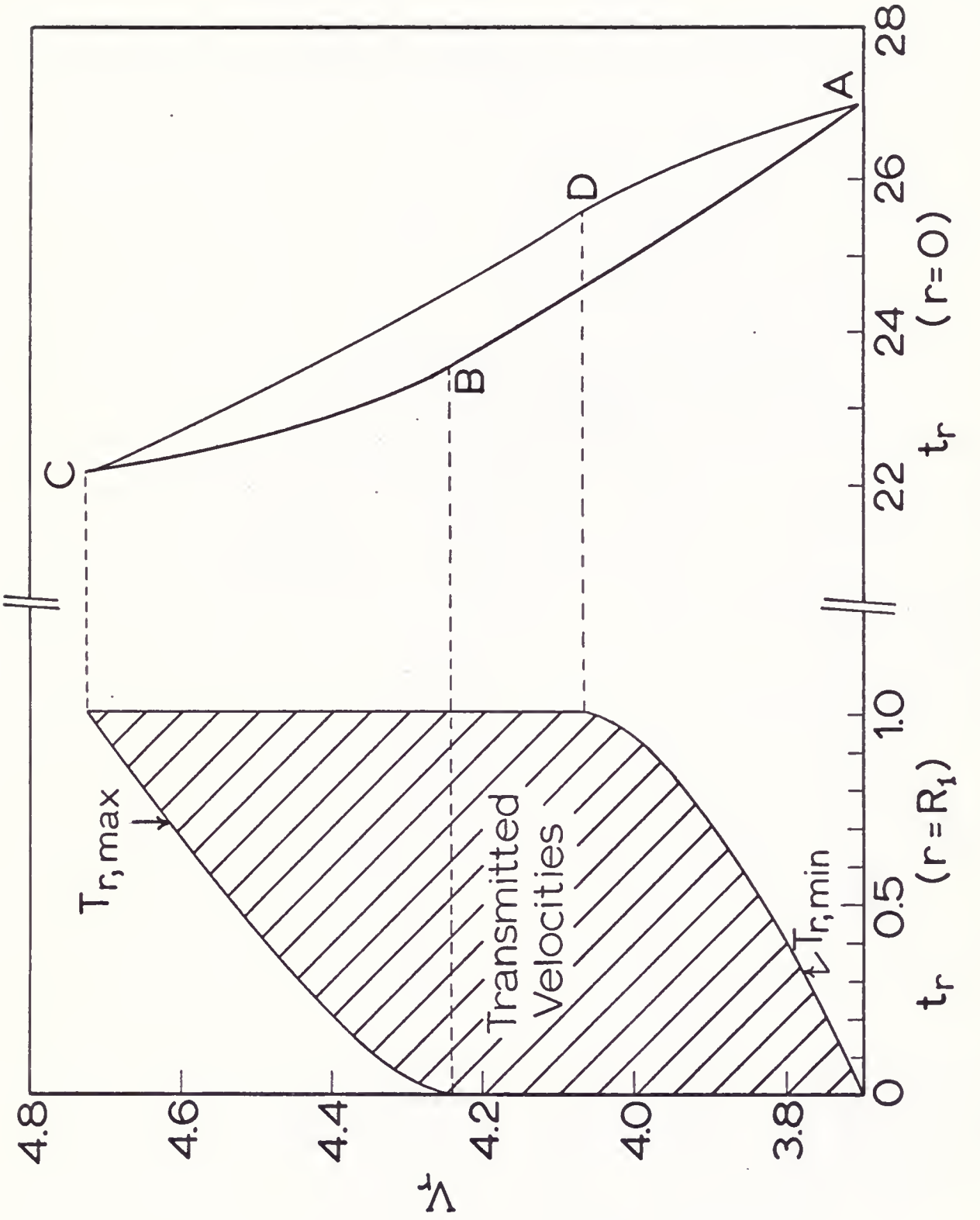
4.8
4.6
4.4
4.2
4.0
3.8
V_r
0
0.5
1.0
t_r (r=R1)
22
24
26
28
t_r (r=0)
A
B
C
D
$T_{r,max}$
$T_{r,min}$
Transmitted Velocities

Fig. 17.-Time dependent transmitted intensities at scattering zone.

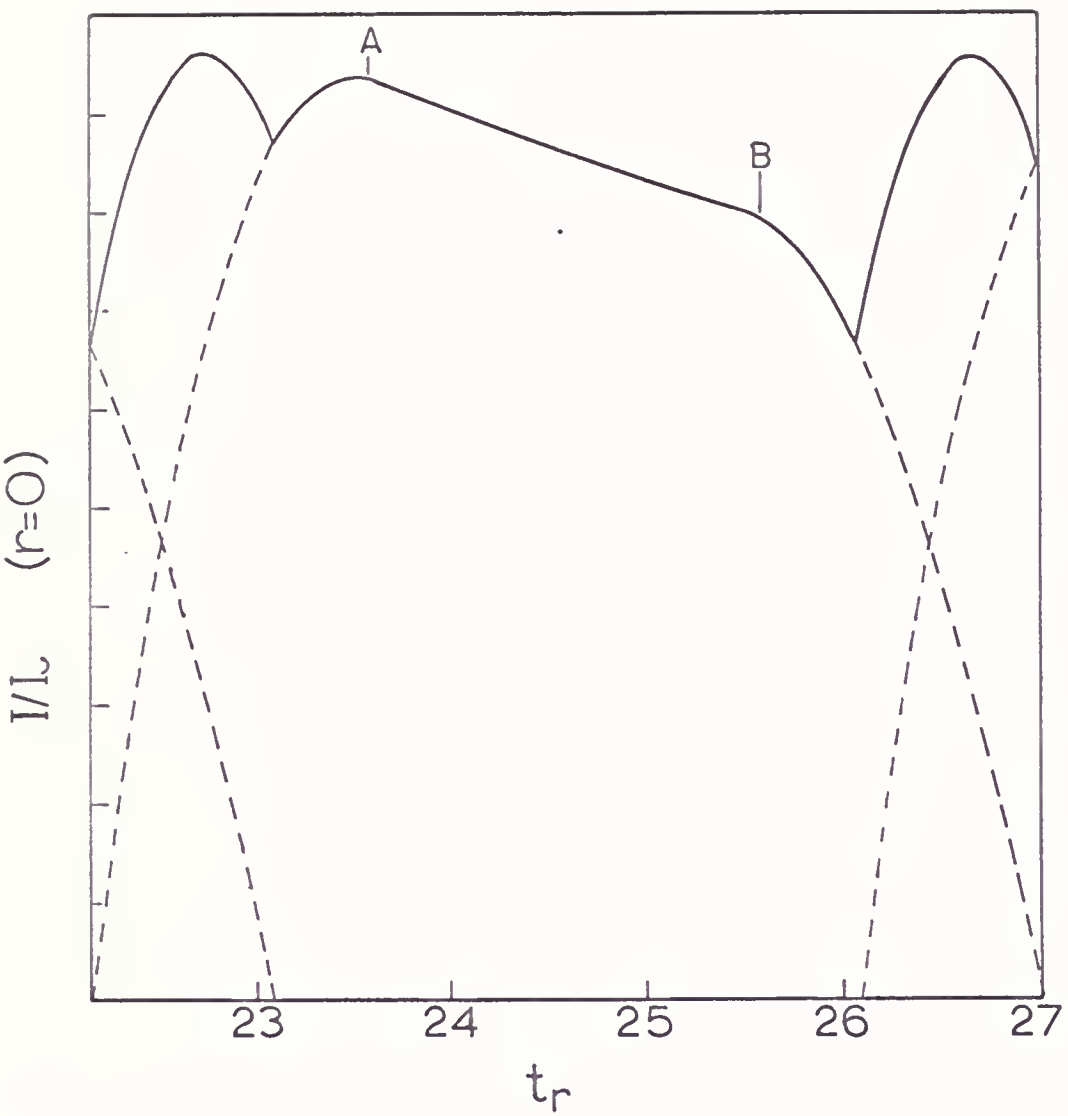
A
B
I/L (r=0)
23
24
25
26
27
t_r

function, $I(V_r)$, of the unselected beam; in the present case $I(V_r)$ is taken to be that which exists in a Maxwellian beam. The transmitted intensity at the scattering center may be found as

$$i_{t_r} = \int_{\Delta V_r(t_r)} I(V_r)dV_r \quad . \tag{29}$$

In terms of Figure 15 a characteristic resolution, ρ, may be defined as

$$\rho = \Delta V_r(f_t = 1/2)/V_{r,M} = R_1\theta_o\Delta V_{r,1/2}/\ell \quad . \tag{30}$$

This treatment of transmission characteristics should be extended further to encompass those particles which arrive at the outer edge of the selector along paths other than normal. This situation will occur in wide or divergent beams. The coordinate system which represents "off normal" transmission is given in Figure 18. Where the angle of incidence of a molecule is γ, its trajectory projected onto the velocity selector is given by

$$\theta_\gamma = (\omega/v)[(R_1^2-h^2)^{1/2} - (r^2-h^2)^{1/2}] + \sin^{-1}(h/r)-\gamma \; ; \tag{31}$$

the angle γ is to be taken as positive or negative as the molecule approaches above or below the horizontal line of Figure 18. The usual approximations may be made in Eqn.

Fig. 18.-Coordinates for transmission of molecules arriving at selector along path striking wheel at angle γ with respect to normal. ϕ_γ is angle through which narrow detector must be moved from beam axis to intercept transmitted molecule.

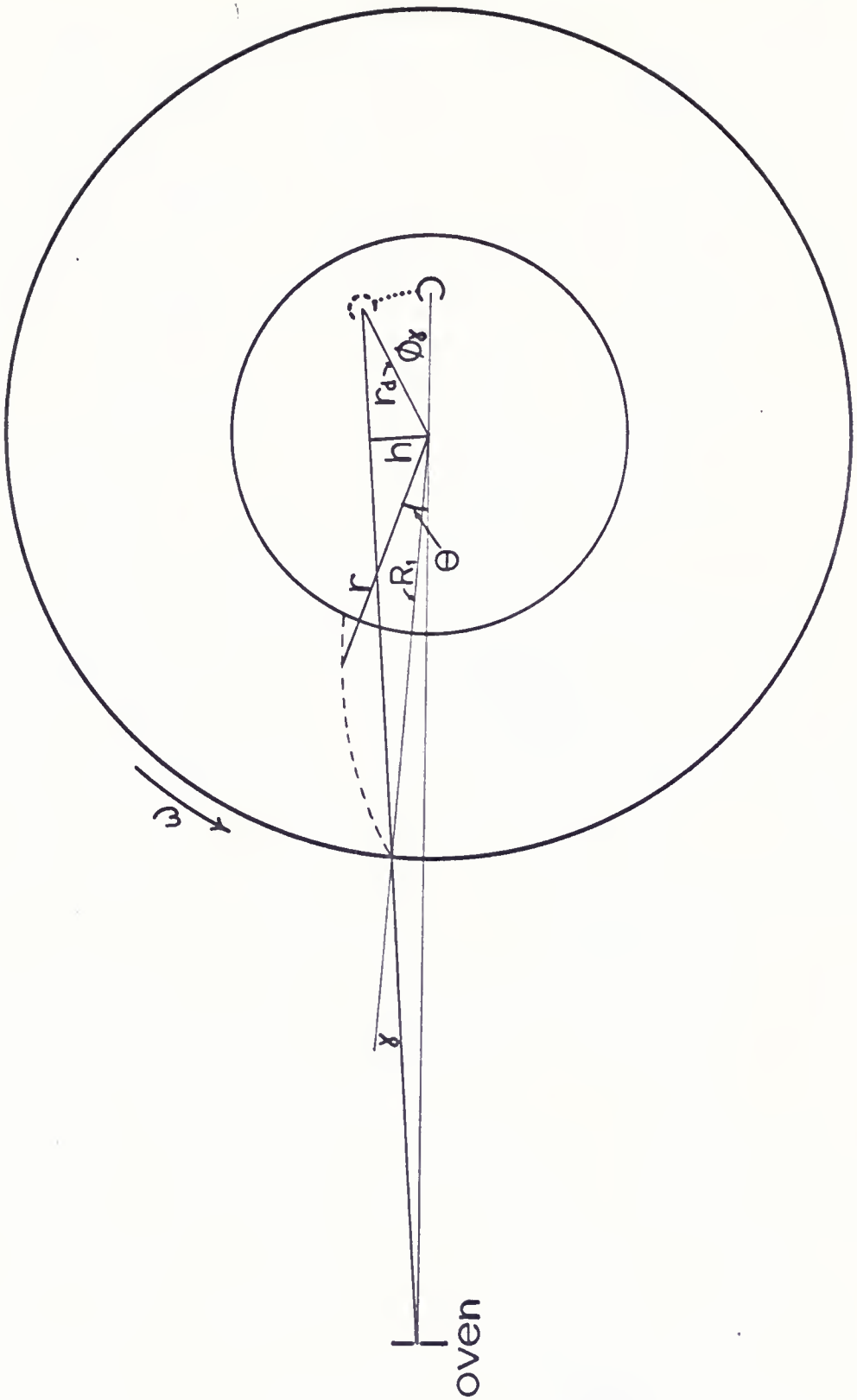
r_d
ϕ_γ
h
d
θ
R_1
r
ω
γ
oven

(31) since the γ's are small and $h << R_2$, consequently

$$\theta_\gamma = (\omega/v)(R_1-r) + (\gamma/r)(R_1-r) \quad . \tag{32}$$

ϕ_γ is the angle through which a narrow detector placed at radial distance r_d must be moved to intercept the molecule.

The transmission equations considering the γ dependence are derived in the same manner as those for normal incidence ($\gamma = 0$). These equations are listed below and have been given the number corresponding to the analogous equation previously given for $\gamma = 0$.

$$r_U = (R_1/2L_v)\left\{ L_v + a(2t_r-1) - \gamma R_1 \pm [(L_v + 2at_r-a-\gamma R_1)^2 \right.$$
$$\left. -4\, L_v(a-\gamma R_1)]^{1/2}\right\} \tag{5a}$$

$$r_L = (R_1/2L_v)\left\{ L_v + a(2t_r-1) - \gamma R_1 \pm [(L_v + 2at_r-a-\gamma R_1)^2 \right.$$
$$\left. +4\, L_v(a+ R_1\gamma)]^{1/2}\right\} \tag{6a}$$

$$L_{v,min,tan} = a(3 - 2t_r) - \gamma R_1 + 2[2a(1-t_r)(a-R_1)]^{1/2}$$
$$R_1 \gg r_{U,tan} \gg R_2 \tag{8a}$$

$$L_{v,max,tan} = -\left\{ a(2t_r + 1) + \gamma R_1 + 2[2at_r(a+\gamma R_1)]^{1/2}\right\}$$
$$R_1 \gg r_{L,tan} \gg R_2 \tag{9a}$$

$$r_{U,tan} = R_1 \left\{a - \gamma R_1 + [2a(1-t_r)(a-\gamma R_1)]^{1/2}\right\} \Big/$$
$$\left\{a(3-2t_r) - \gamma R_1 + 2[2a(1-t_r)(a-\gamma R_1)]^{1/2}\right\} \tag{10a}$$

$$r_{L,tan} = R_1 \left\{ a + \gamma R_1 + [2at_r(a+\gamma R_1)]^{1/2} \right\} / \left\{ a(2t_r+1) + \gamma R_1 + 2[2at_r(a+\gamma R_1)]^{1/2} \right\} \quad (11a)$$

$$T_{r,max} = (a+\gamma R_1)\, \ell^2 / 2aR_2^2 \quad (12a)$$

$$L_{v,min,ob} = (R_1\, a/\ell)\, [(R_1+R_2)/R_2 - 2t_r - \ell\gamma R_1/R_2]$$

$$t_r < T_{r,min} \quad (13a)$$

$$L_{v,max,ob} = -(R_1\, a/\ell)\, [\ell/R_2 + 2t_r + \ell\gamma R_1/R_2]$$

$$t_r > T_{r,max} \quad (14a)$$

$$V_{r,min,ob} = \ell[\theta_o R_1 + a(R_1+R_2)/R_2 - 2at_r - \ell\gamma a\, R_1/R_2]^{-1}$$

$$0 < t_r < T_{r,min} \quad (15a)$$

$$V_{r,min,tan} = \ell\{\theta_o R_1 - (\ell/R_1)(a(3-2t_r) - \gamma R_1 + 2[2a(1-t_r)(a-\gamma R_1)]^{1/2})\}^{-1} \quad T_{r,min} \leqslant t_r \leqslant 1 \quad (16a)$$

$$V_{r,max,tan} = \ell\{\theta_o R_1 - (\ell/R_1)(a(2t_r+1) + \gamma R_1 + 2[2at_r(a-\gamma R_1)]^{1/2}\}^{-1} \quad 0 \leqslant t_r \leqslant T_{r,max} \quad (17a)$$

$$V_{r,max,ob} = \ell[\theta_o R_1 - a\,\ell/R_2 - 2at_r - \gamma a\,\ell\, R_1/R_2]^{-1}$$

$$T_{r,max} \leqslant t_r \leqslant 0 \quad (18a)$$

$$f_t(V_r) = t_r = R_1\theta_o/2a + (R_1+R_2)/2R_2 - \ell\gamma R_1/R_2 - \ell/2aV_r$$

$$V_1 \leqslant V_r \leqslant V_2 \quad (19a)$$

$$f_t(V_r) = t_r = (1/2)[1 + \gamma R_1/a - (R_1/a)(1/V_r - R_1\theta_o/\ell\,)] + [(1+\gamma R_1/a)(R_1/a)(1/V_r - R_1\theta_o/\ell\,)]^{1/2}$$

$$V_2 \leqslant V_r \leqslant V_3 \qquad (20a)$$

$$f_t(V_r) = (1-t_r) = (1/2)[1 + 3\gamma R_1/a + (R_1/a)(1/V_r - R_1\theta_o/\ell\,)] + \left\{(1+\gamma R/a)(R_1\theta_o/\ell - 1/V_r) + 2\gamma R_1/a\right\}^{1/2}$$

$$V_4 \leqslant V_r \leqslant V_5 \qquad (22a)$$

$$f_t(V_r) = (1-t_r) = -R_1\theta_o/2a + \ell/2aV_r + (R_1+R_2)/2R_2 + \ell\gamma R_1/2R_2$$

$$V_5 \leqslant V_r \leqslant V_6 \qquad (23a)$$

The total transmitted intensity of a molecular beam effusing through a narrow slit and incident on a narrow detector at a position ϕ_γ is

$$I_{\omega,\gamma} = n\omega/2\pi \int_{V_1}^{V_6} f_\gamma(V_r) I_\gamma(V_r) dV_r \ldots \qquad (26a)$$

B. Collision Theory[42-46]

Before describing the quantum mechanical treatment of elastic atomic collisions, the classical representation should be considered in some detail. This will afford certain concepts to which aspects of the quantum treatment can be referred.

The assumption will be made that molecules can be represented as point centers of force and, in addition, that they interact in pairs with conservative forces along lines joining their centers. For the present, consideration will be given to collisions that occur between a constant speed molecular beam and a fixed target molecule. Generalizations to actual situations will be discussed later.

Consider a homogeneous beam of particles moving along paths that are parallel but otherwise distributed at random. Let this beam pass over a particle held in a fixed position. If attention is now drawn to the fraction of particles that undergo a particular deflection by the target particle, then a quantity G may be defined such that the fraction of incident particles which are deflected into a solid angle $d\omega$ is given by $Gd\omega$. G is called the scattering coefficient or differential scattering cross-section. It will, in general, vary with the direction of scattering and, consequently, should be denoted in polar coordinates as $G(\theta,\phi)$.

As a rule a more useful quantity is the polar scattering coefficient, $F(\theta)$. This quantity represents the fraction of beam particles incident on a unit area which are scattered by one scattering center through angles θ and $\theta + d\theta$. Consequently all particles scattered (by a spherically symmetric potential) into the range $d\theta$ are

represented by $G(\theta)d\omega = 2\pi\, G(\theta)\sin\theta d\theta = F(\theta)d\theta$.

The total collision cross-section, S, is the total fraction of beam particles per unit area removed from the beam by collision with one scattering center. Therefore

$$S(\theta) = \int_0^{\pi} F(\theta)d\theta = 2\pi \int_0^{\pi} G(\theta)\sin\theta d\theta \ . \qquad (33)$$

The quantity measured experimentally is given by

$$S(\theta') = \int_{\theta'}^{\pi} F(\theta)d\theta = 2\pi \int_{\theta'}^{\pi} G(\theta)\sin\theta d\theta \ . \qquad (34)$$

This last equation results from the fact that all detectors must have a finite width; thereby not allowing detection of scattering through angles less than θ' .

The classical scattering coefficient may now be used to calculate the collision cross-section for any spherically symmetrical type of force between beam particles and a fixed scatterer. Because of the interaction force the beam molecule will be deflected so as to move along a plane curve (Figure 19) (this case being for a repulsive force; for an attractive force the orbit would curve the other way). The collision parameter, b, is merely the distance of closest approach assuming no interaction takes place. The net deflection is denoted by the angle θ and the distance of closest approach by r_o. At any instant the position of the molecule is given by the polar angle, ϕ, and the distance from the scattering center, r .

Fig. 19.-Classical orbit of a particle moving with velocity v through an isotropic repulsive force field originating at a fixed point: b-impact parameter, r and ϕ - coordinates of particle, r_o - distance of closest approach, θ - deflection angle.

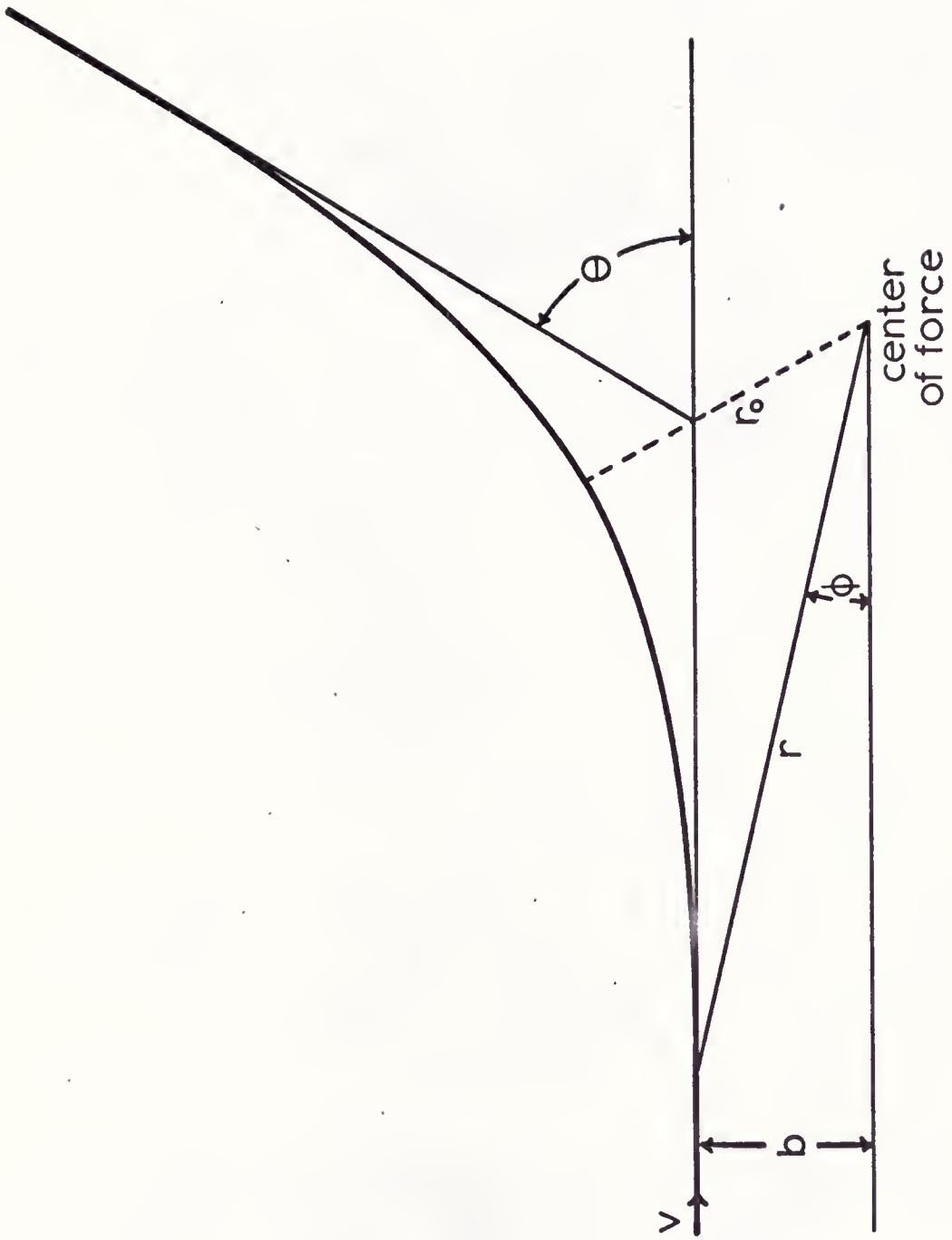
Θ
r_o
center
of force
φ
r
b
v

Let m be the mass of the molecule so that at any instant its angular momentum and kinetic energy are given by $mr^2\dot{\phi}$ and $m(\dot{r}^2 + r^2\dot{\phi}^2)/2$ respectively.[47] The initial values of the latter quantities are mvb and $mv^2/2$; so that by conservation of angular momentum and energy there results:

$$mvb = mr^2\dot{\phi} \tag{35}$$

$$mv^2/2 = m(\dot{r}^2 + r^2\dot{\phi}^2)/2 + V(r) \tag{36}$$

where V(r) is the potential energy between the interacting particles. Solving the above two equations for $\dot{\phi}$ and $\dot{r}$, one obtains

$$d\phi/dr = b[\,1 - 2V(r)/mv^2 - (b/r)^2]^{-1/2}/r^2 \,. \tag{37}$$

The total change in ϕ during the collision is $\pi - \Theta$, or since the orbit is symmetrical about the point of closest approach,

$$\pi - \Theta = 2 \int_{r_o}^{\infty} (d\phi/dr)dr \tag{38}$$

This allows calculation of the net deflection Θ, as a function of b,

$$\Theta(b) = \pi - 2b \int_{r_o}^{\infty} r^{-1}\left\{ (1-2V(r)/mv^2)r^2 - b^2 \right\}^{-1/2} dr \,. \tag{39}$$

Paths of approach taken by particles in the beam on the average are directed uniformly over a plane perpendicular

to their direction. Consequently the fraction of molecules in the beam with impact parameters between b and b + db are scattered into a range $d\theta$; so that $d\theta = \theta(b)db$ and $F(\theta) = 2\pi b/\theta(b)$. This then allows the calculation of the total scattering cross-section, for a given scattering potential, from Eqn. (33).

The general treatment of scattering must consider the motion of the target particles and the distribution of velocities present in the beam. The physical situation can be related to the discussion by dividing this effect into two parts: one arising from the initial motion of the scattering particle, and the second from the acceleration of the scattering molecule during collision. The first effect is dealt with by considering the relative motions of the interacting particles and performing an appropriate averaging over all the relative motions. The second effect is understood by considering the fact that when two particles move under the action of mutual forces, the motion of one relative to the other is the same as would be its actual motion if the second one were held fixed and the first ones mass reduced to $m_1 m_2/(m_1+m_2)$.

In a number of experimental conditions a problem arises with the use of classical mechanics to describe the differential scattering cross-section. This results from the divergence of $G(\theta)$ for all force fields which extend to

infinity. For such fields as these there is no upper limit to the impact parameter. All deflections are counted no matter how large the impact parameter. This generates an effective scattering area for a particle which is infinite. If quantum mechanics is used to describe the scattering process, there will exist a range beyond which the deflection of a scattered particle will be less than the uncertainty of its position and momentum; consequently the particle will not be considered to have undergone any interaction with the scattering center. It is the problem, divergence of the classical differential scattering cross-section for small angles, that requires a quantum mechanical treatment to describe the scattering process in most experimental cases.

In order to treat the scattering problem quantum mechanically the fact that the motion of particles can not be described with complete accuracy must be taken into account. Wave packets are used from whose average coordinates arise the classical orbits. The determination of collision cross-sections must resolve itself into finding solutions to the Schroedinger wave equation,

$$-(\hbar^2/2u)\nabla^2\psi + V(r)\psi = E\psi \quad . \tag{40}$$

This equation represents a particle of mass u and kinetic energy E moving through a scattering potential of V(r).

Equation (40) may be transformed into one involving the wave number $k = \mu v/\hbar$, of the particle undergoing scattering,

$$\nabla^2\psi + (k^2-U)\psi = 0 \qquad (41)$$

where

$$U = 2\mu V(r)/\hbar^2 .$$

Scattering is determined by the asymptotic form of the wave function,

$$\psi(r,\theta) \underset{r\to\infty}{=} A[\exp(ikz) + f(\theta)\exp(ikr)/r] , \qquad (42)$$

which is a solution to the above wave Eqn. (33) and assumes the action of a spherically symmetrical potential with the z axis as the direction of incidence of the beam. Here A is a normalization constant. The term $A[\exp(ikz)]$ represents a plane wave incident on the scattering center, while the second term in (42) represents an outgoing spherical wave; for a spherically symmetric potential the amplitude of the scattered wave depends only on the polar angle θ and is inversely proportional to r . The incident beam flux is given by $v|A|^2$ whereas the scattered flux along an outward radius is given by $v|A|^2|f(\theta)|^2/r^2$. Then by definition the differential scattering cross-section is:

$$G(\theta) = |f(\theta)|^2 . \qquad (43)$$

Although the asymptotic behavior of the wave function determines the scattering cross-section, it can not be found unless the wave equation is solved for all space. There are two generally accepted means for obtaining solutions: the method of partial waves and an integral equation method. The former method will be discussed here.

The general solution to the wave Eqn. (33) consists of an infinite sum of Legendre polynomials

$$\psi(r,\theta) = \sum_{\ell=0}^{\infty} R_\ell(r)P_\ell(\cos\theta) \tag{44}$$

where ℓ is the angular momentum quantum number. Provided the potential energy V(r) has a more rapid decrease than 1/r the general solution can take the asymptotic form,

$$\psi(r,\theta) \xrightarrow[r\to\infty]{} (kr)^{-1} \sum_{\ell=0}^{\infty} (2\ell+1)\exp[i(\ell\pi/2 + \delta_\ell)]P_\ell$$

$$(\cos\theta)\sin(kr - \ell\pi/2 + \delta_\ell) \tag{45}$$

The angle δ_ℓ is called the phase shift of the ℓ^{th} partial wave. It is the difference in phase between the actual radial function $R_\ell(r)$ and the radial wave function in the absence of a scattering potential (V(r)=0). A repulsive potential implies a decrease in the relative velocity of the interacting particles thus increasing the wavelength; therefore, the scattered wave is "pushed out" relative to that

for $V(r)=0$ and suffers a negative phase shift. The effect is opposite for an attractive potential and the wave is "pulled in" producing a positive phase shift.

The amplitude of the scattered wave may be expressed as a function of the phase shift:

$$f(\theta)\exp(ikr)/r = (kr)^{-1} \sum_{\ell=0}^{\infty} (2\ell+1)\exp(i\ell\pi/2)$$

$$[\exp(i\delta_\ell)\sin(kr-\ell\pi/2+\delta_\ell)-\sin(kr-\ell\pi/2)]P_\ell(\cos\theta) \tag{46}$$

or

$$f(\theta) = (2ik)^{-1} \sum_{\ell=0}^{\infty} (2\ell+1)[\exp(2i\delta_\ell)-1]P_\ell(\cos\theta) .$$

Therefore the differential scattering cross-section becomes:

$$G(\theta) = (k^2)^{-1} \left| \sum_{\ell=0}^{\infty} (2\ell+1)\exp(i\delta_\ell)\sin\delta_\ell P_\ell(\cos\theta) \right|^2 , \tag{47}$$

and the total scattering cross-section is given by

$$S(0) = 2\pi \int_0^{\pi} G(\theta)\sin\theta d\theta = (4\pi/k^2) \sum_{\ell=0}^{\infty} (2\ell+1)\sin^2\delta_\ell . \tag{48}$$

All that remains is the calculation of the phase shifts δ_ℓ. If a spherically symmetrical potential of the form $V(r) = C/r^s$ $(s > 3)$ is employed application of the JWKB approximation gives:

$$\delta_\ell \approx \int_a^\infty \left\{1-[(\ell+1/2)/kr]^2 - U/r^2\right\}^{1/2} dr - k \int_{(\ell+1/2)/k}^\infty \left\{1-[(\ell+1/2)/kr]^2\right\}^{1/2} dr \,, \qquad (49)$$

where the lower limit of each integral is the zero of the integrand. The limit $\underline{a}$ is the analog of the classical distance of closest approach. Also the limit $(\ell + 1/2)/k$ is the analog of the classical impact parameter. For large ℓ Eqn. (49) may be simplified because $\underline{a}$ is also large and approximately equal to $(\ell + 1/2)/k$. The value of V(r) is necessarily small and the first integrand may be expanded in a binomial series and the two integrals combined to yield

$$\delta = (\mu C/\hbar^2) \int_{\ell/k}^\infty [k^2 - \ell^2/r^2]^{-1/2} r^{-s} dr \qquad (50)$$

where $(\ell + 1/2)$ has been replaced by .

If the sum in Eqn. (48) is replaced by an integral, then

$$S(0) = (8\pi/k^2) \int_0^\infty \sin^2\delta_\ell \, d\ell \,. \qquad (51)$$

Upon performing the integration the total scattering cross-section becomes,

$$S(0) = 2\pi^{s/(s-1)} \sin\left[\frac{(\pi/2)(s-3)}{(s-1)}\right]\left\{\Gamma\left[\frac{s-3}{s-1}\right]\left[\frac{\Gamma(s/2-1/2)}{\Gamma(s/2)}\right][C/(h\,v)]\right\}^{2/(s-1)} . \qquad (52)$$

This is the Landau and Lifshitz equation.

The point of transition between the classical and quantum mechanical treatment of the scattering process should now be considered.

For comparison consider a situation in which the deflection of a scattered particle is χ ; with this particle having a mass μ, velocity v, and experiencing a potential field of the order V confined to dimensions of the order a. In order for the classical description of scattering to hold two conditions must be satisfied. First, the uncertainty in the position of the particle while experiencing deflection must be small compared to a. Second, the angle of deflection produced by scattering must be well defined.

If the first condition is satisfied then there must be an uncertainty in the momentum of the particle of $\hbar/a$ or larger. In order for classical mechanics to remain valid then $\hbar/a \ll \mu v$, or in a more familiar form,

$$\lambda \ll a \quad . \tag{53}$$

The deflection is determined by the momentum transfer, therefore the second condition requires that $\hbar/a \ll V/v$ or that

$$\lambda/a \ll \chi \quad . \tag{54}$$

Both Eqns. (53) and (54) must be realized in order for classical mechanics to describe the scattering process. This is usually achieved only in scattering experiments involving high energy beams and a thermal target gas or in cases of extremely low resolution scattering experiments.

In almost all other cases the quantum description of scattering must be used because either one or both of the above conditions fails to be met.

IV. RESULTS AND DISCUSSION

A. Measurement of Transmission

The transmission characteristics of a parallel wall, spiral groove velocity selector described in the previous section will be compared to the measured intensities of velocity selected beams of cesium (these measurements taken in the manner previously described). If this comparison is to be meaningful, the distribution function, $I(V_r)dV_r$, for intensities in the unselected beam must be precisely known. Conditions for effusive flow through the oven slits are well satisfied; consequently it may be assumed that the distribution of Cs vapor velocities inside the oven is Maxwellian. The distribution function for intensities in the unselected Maxwellian beam is given in terms of reduced velocity by[48]

$$I(V_r)dV_r = 2I_o(R_1\omega/\alpha)^4 V_r^3 \exp(-R_1\omega V_r/\alpha)^2 dV_r \quad (55)$$

where I_o is the intensity of the unselected beam and $\alpha = (2kT/m)^{1/2}$ and m is the molecular mass. This expression is seen to exhibit a V_r^3 dependence rather than the familiar V_r^2 dependence for the Maxwellian distribution in a gas at equilibrium. The V_r^3 dependence results because the probability of a particle moving through the slit is

proportional to the particle's velocity. Considering now the case of $\gamma = 0$, substitution of Eqn. (55) into Eqn. (25) and the evaluation of the definite integral permits calculation of I_ω from Eqn. (26). A problem arises, however, in the evaluation of the integral over the tangentially limited velocity ranges $V_2 \rightarrow V_3$ and $V_4 \rightarrow V_5$; these integrals could not be reduced because of the radicals in Eqns. (20) and (22). It was found that these two functions could be approximated within 1 per cent with quadratics of the form

$$f_t(V_r) = C_1 + C_2 V_r + C_3 V_r^2 \qquad (56)$$

and the integrals evaluated. The resulting expression for transmitted intensity is

$$\begin{aligned} I_\omega = (n\omega I_o/2\pi) \; \{ & \langle [a(R_1 + R_2) - \ell R_1 \, a + \theta_o R_1 R_2]/2aR_2 \rangle \\ & [(Y_1^2 + 1)E_1 - (Y_2^2 + 1)E_2]S + (\ell/2a)[Y_2 E_2 - Y_1 E_1 \\ & + (\pi^{1/2}/2)(ERF_1 - ERF_2)] + C_1[(Y_2^2 + 1)E_2 - \\ & (Y_3^2 + 1)E_3]S + C_2[(Y_2^3 + 3Y_2/2)E_2 - (Y_3^3 + \\ & 3Y_3/2)E_3 + (3\pi^{1/2}/4)(ERF_3 - ERF_2)]S^2 + \\ & C_3[Y_2^4 + 2Y_2^2 + 2)E_2 - (Y_3^4 + 2Y_3^2 + 2)E_3]S^3 + \\ & [(Y_3^2 + 1)E_3 - (Y_4^2 + 1)E_4]S + C_1'[(Y_4^2 + 1)E_4 - \\ & (Y_5^2 + 1)E_5]S + C_2'[(Y_4^3 + 3Y_4/2)E_4 - (Y_5^3 + 3Y_5/2)E_5 + \end{aligned}$$

$$(3\pi^{1/2}/4)(ERF_5 - ERF_4)]S^2 + C_3'[(Y_4^4 + 2Y_4^2 + 2)E_4 - (Y_5^4 + 2Y_5^2 + 2)E_5]S^3 + \langle[a(R_1 + R_2) - R_1R_2\theta_o + R_1 a]/2aR_2\rangle [(Y_5^2 + 1)E_5 - (Y_6^2 + 1)E_6]S + (\ell/2a)[Y_5E_5 - Y_6E_6 + (\pi^{1/2}/2)(ERF_6 - ERF_5)]\} \quad , \tag{57}$$

where

$$S = \alpha/R_1\omega \quad , \tag{58}$$

$$Y_i = V_i/S \quad , \tag{59}$$

$$E_i = \exp(-Y_i^2) \quad , \tag{60}$$

and

$$ERF^{49} = (2/\pi^{1/2}) \int_0^{Y_i} \exp(-x^2)dx \ . \tag{61}$$

I_ω is plotted as the dashed line in Figure 20, along with the experimental points. These curves are normalized to agree at the maximum transmitted intensity. The experimental points are in good agreement with the theoretical curve over a major portion of the distribution; however there is a deficiency of observed atoms in the low velocity region. Similar deficiencies at low velocities observed in previous experiments[21,23] have been attributed to velocity dependent attenuation of the beam due to collisions in the neighborhood of the oven slit. In the present case very low oven pressures are used, and essentially ideal slits are employed; therefore, it is believed that the

Fig. 20.-Transmission of narrow beam of cesium atoms effusing from oven at 405°K and entering selector at normal incidence; comparison of experimental values with theoretical expressions for a beam transmitted both with and without attenuation due to residual background gases.

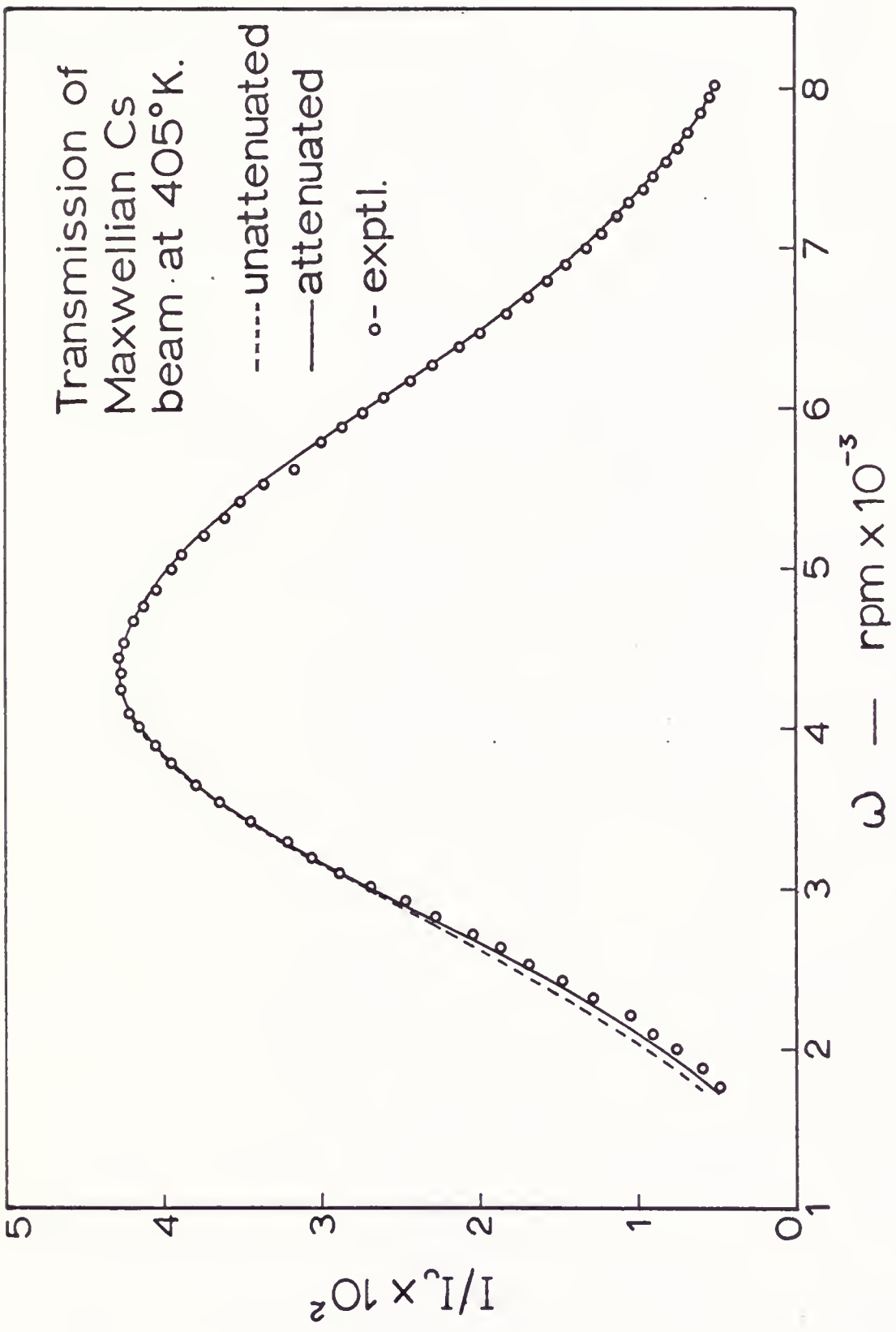
Transmission of
Maxwellian Cs
beam at 405°K.
----unattenuated
——attenuated
o- exptl.
I/I$_0$ x 10^2
0
1
2
3
4
5
1
2
3
4
5
6
7
8
ω — rpm x 10^{-3}

deficiency results mainly from attenuation of the beam due to scattering by the background gases.

The above effect can be evaluated by considering the probability P(v) that a beam molecule with speed v will reach the detector without undergoing a collision with a background molecule,

$$P(v) = \exp(-\ell_1/\lambda_{v1} - \ell_2/\lambda_{v2}) \tag{62}$$

where λ_{v1} and λ_{v2} are the mean free paths of beam molecules in the beam and selector chambers, respectively. The expression for λ_v for a molecule moving with velocity v through a Maxwellian gas of number density n_G and $\alpha_G = (2kT_G/m_G)^{1/2}$ is given by[50]

$$\lambda_v = \pi^{1/2}(v/\alpha_G)^2/n_G\,\bar{\sigma}\,\psi(v/\alpha_G) \tag{63}$$

where $\bar{\sigma}$ is the mean effective cross-section for the scattering of the beam molecule by the gas, and $\psi(x)$ is defined as

$$\psi(x) = x\exp(-x^2) + (2x^2 + 1)\int_0^x \exp(-y^2)dy \tag{64}$$

There are two methods for arriving at the background attenuated, transmitted intensity; both use the integral

$$I_\omega = (n\omega/2\pi)\int_{\Delta V_r} f_t(V_r)P(V_r)I(V_r)dV_r \tag{65}$$

as a point of departure. The first method involves the evaluation of the above integral using the cross-section

as a parameter which is adjusted to obtain the best fit of the experimental points. The second method involves various approximations introduced in Eqn. (65) by considering the transmission of a Maxwellian beam through a velocity selector having narrow groove widths. The narrow groove will transmit velocities in a small range centered about $v_m = \ell\omega/\theta_o$, with the transmission profile (Figure 15) approaching a step function of height $f_t = 1$. The approximations introduced by considering a narrow groove are: $f_t(V_r) = 1$, $V_r = v_m/R_1\omega = \ell/R_1\theta_o$, and $dV_r = \Delta V_r = \rho'\ell/R_1\theta_o$, where ρ' is an effective resolution. Introducing these approximations in Eqns. (55), (62), and (63) permits the above integral to be expressed as

$$I_\omega = (I_o an\rho'/R_1\pi)X_B^4 \exp(-X_B^2) \times \left\{ \exp[-\ell' n_G' \bar{\sigma} \psi(X_G) / \pi^{1/2} X_G^2] \right\} \qquad (66)$$

where

$$X_B = \ell\omega/\alpha\theta_o \qquad (67)$$

$$X_G = \ell\omega/\alpha_G\theta_o$$

and

$$\ell' n_G' = \ell_1 n_{G1} + \ell_2 n_{G2} \quad , \qquad (68)$$

where n_{G1} and n_{G2} are the number densities of background molecules in the beam and velocity selector chambers, respectively. This latter method for obtaining the

attenuated I_ω's because of its simplicity was chosen over the former one.

From Eqn. (66) it is seen that the unattenuated ($n_G = 0$) transmitted intensity for a narrow groove selector should be

$$I_\omega = (I_\upsilon a n \rho'/R_1 \pi) X_B^4 \exp(X_B^2) \qquad (69)$$

Therefore, the narrow groove approximation is valid if a plot of $\ln (I_\omega/I_\upsilon \omega^4)$ versus ω^2, for the theoretical unattenuated transmitted intensities of the actual velocity selector, approaches a straight line. Figure 21 is such a plot, the average deviations of the points from the linear least squares fit is 0.113 per cent. The slope of the line is -9.1939×10^{-6} sec^2 whereas the theoretical value $-(\ell/a\theta_0)^2$ is 9.270×10^{-6} sec^2. From the intercept, $\ln[a n \rho'/R_1 \pi)\ (\ell/\alpha\theta_0)^4] = -25.6435$, ρ' is found to be 0.173. This is slightly less than the empirically determined resolution, 17.8 per cent; however because of the extremely good fit to a straight line 17.3 per cent can be taken as the actual resolution.

The calculation of the attenuated I_ω's from Eqn. (58) requires a value of $\bar{\sigma}$; this is obtained from the slope $(-\ell' n'_G \bar{\sigma}/\pi^{1/2})$ of the plot $[\ln(I_\omega/I_\upsilon X_B^4) + X_B]^2$ versus $\psi(X_B)/X_B^2$ (Figure 22) for the experimental I_ω's. A least squares fit to the points in this plot yields a straight

Fig. 21.-Theoretical transmission of narrow Maxwellian cesium beam showing close approximation of behavior of present selector to that of one with very narrow grooves.

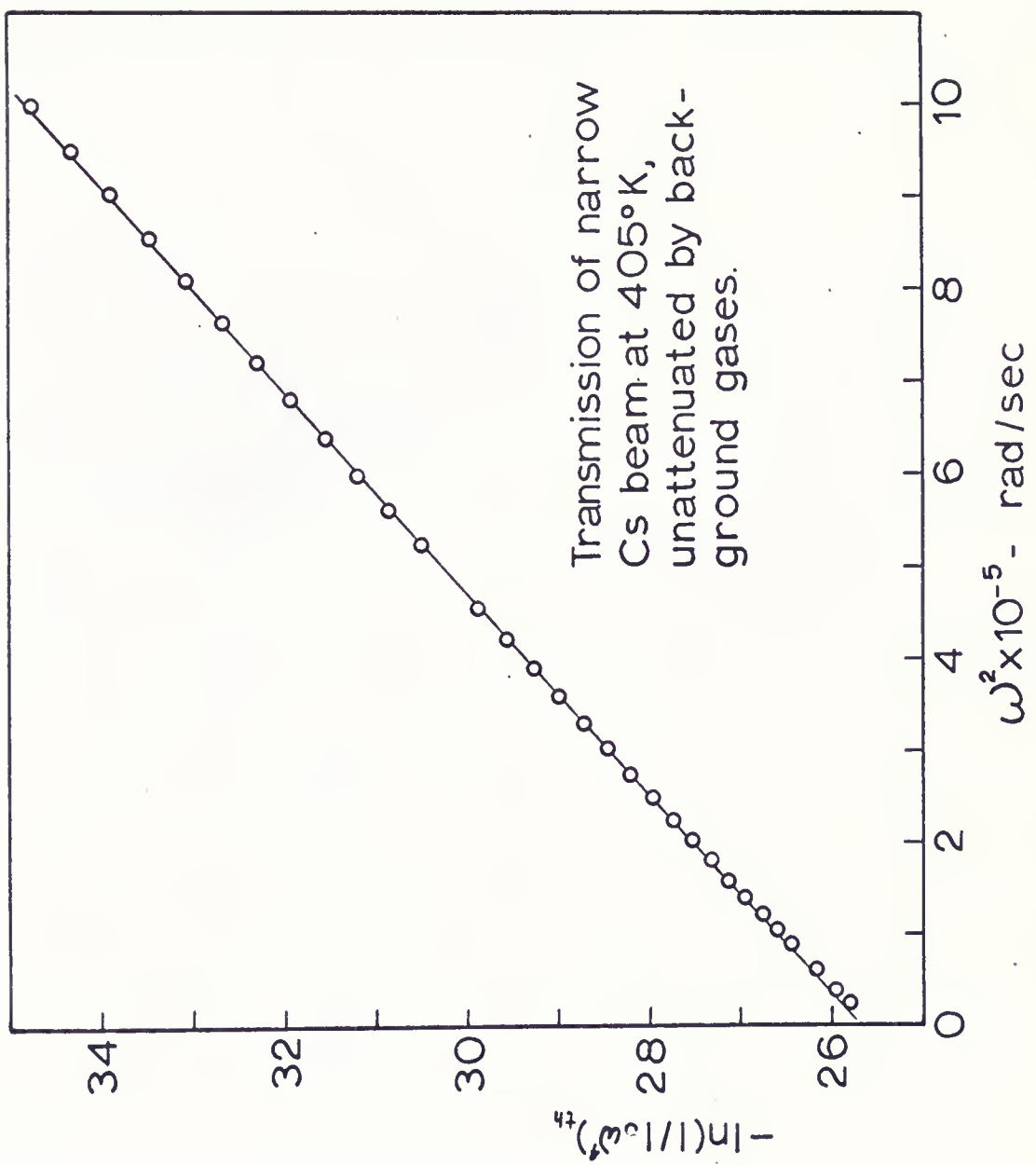
Transmission of narrow
Cs beam at 405°K,
unattenuated by back-
ground gases.
$-\ln(I/I_0\varepsilon')_{47}$
$\omega^2 \times 10^{-5}$ - rad/sec
26
28
30
32
34
0
2
4
6
8
10

Fig. 22.-Plot of experimental data used to determine correction of the theoretical transmitted intensities for attenuation of the cesium beam by scattering in the residual background gases (air). The straight line is determined by method of least squares.

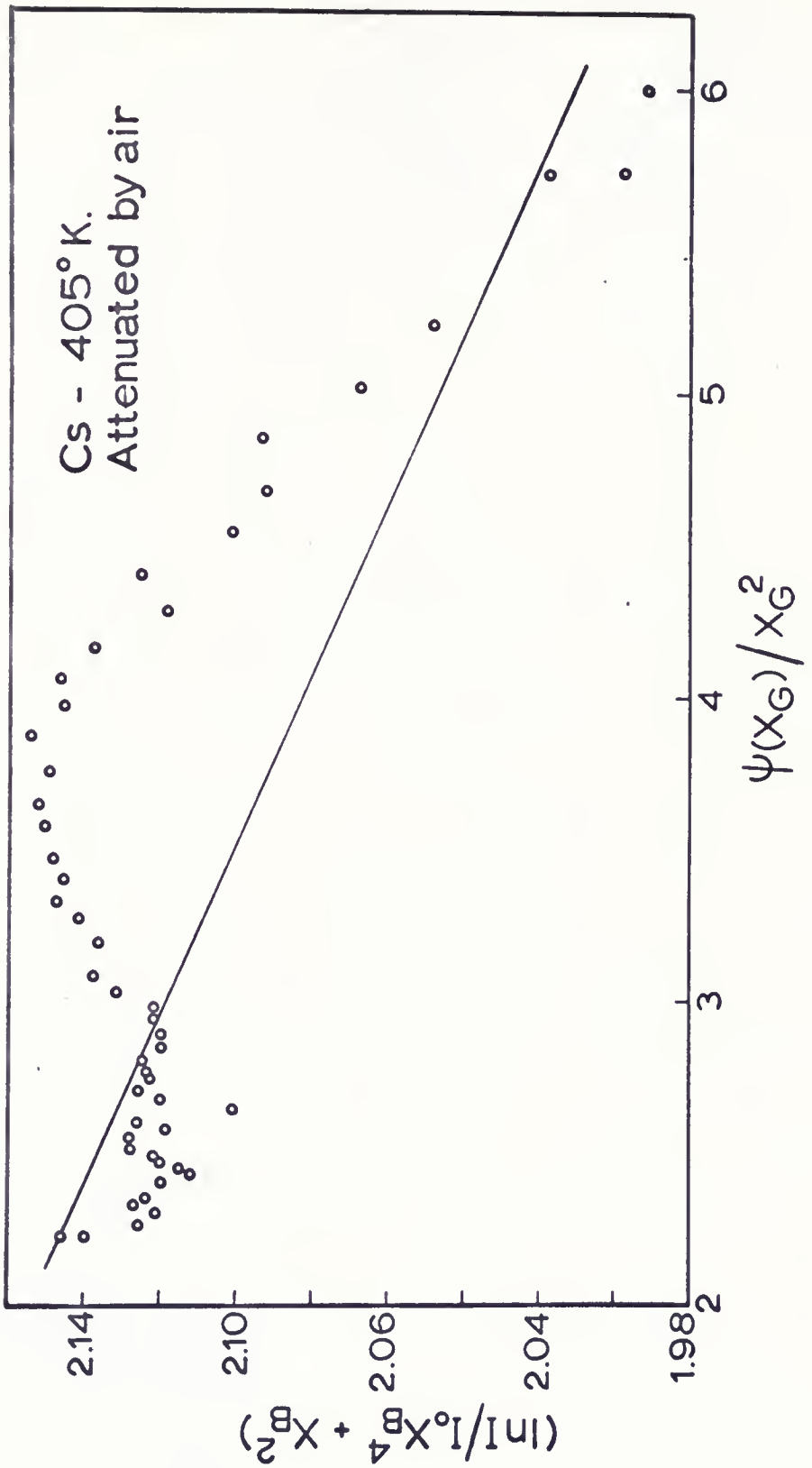
Cs - 405° K.
Attenuated by air
$(\ln I/I_0 X_B^4 + X_B^2)$
2.14
2.10
2.06
2.04
1.98
2
3
4
5
6
$\psi(X_G)/X_G^2$

line whose average deviation is 1.1 per cent and whose slope is 0.03002. The attenuated I_ω's calculated using this value of the slope are shown as the solid line in Figure 20. The average deviation of the experimentally determined I_ω's from this line is 3.1 per cent.

As a further test of the validity of this treatment the average cross-section $\bar{\sigma}$ can be calculated. A problem arises, however, in assigning values to n_{G1} and n_{G2}. The pressures given in Table 1 are obtained with ion gauges; consequently their reliability is somewhat in doubt. Nevertheless the value calculated for $\bar{\sigma}$ using these pressures is 465 $\mathring{A}^2$ which surprisingly enough compares very well to the average Cs - N_2 cross-section obtained in the next section.

From Eqn. (26a) the transmitted beam intensity, $I_{\omega,\gamma}$, for angles of incidence other than zero can be calculated. Figure 23 illustrates the effect of γ on the transmitted intensity for several angular speeds of the velocity selector. This plot demonstrates that for beam particles of a particular mass and temperature there is only one angular speed of the selector for which maximum transmission occurs at the angle $\gamma = 0$. As an experimental check of these transmission characteristics, the transmitted beam intensities as functions of the detector angle ϕ_γ were taken for selector speeds of 189 rad./sec. and 844 rad./sec. These speeds correspond to transmission

Fig. 23.-Calculated values of the reduced transmitted intensities as functions of incidence angle γ of a narrow Maxwellian beam of Cs atoms (405°K) at various selector speeds ω .

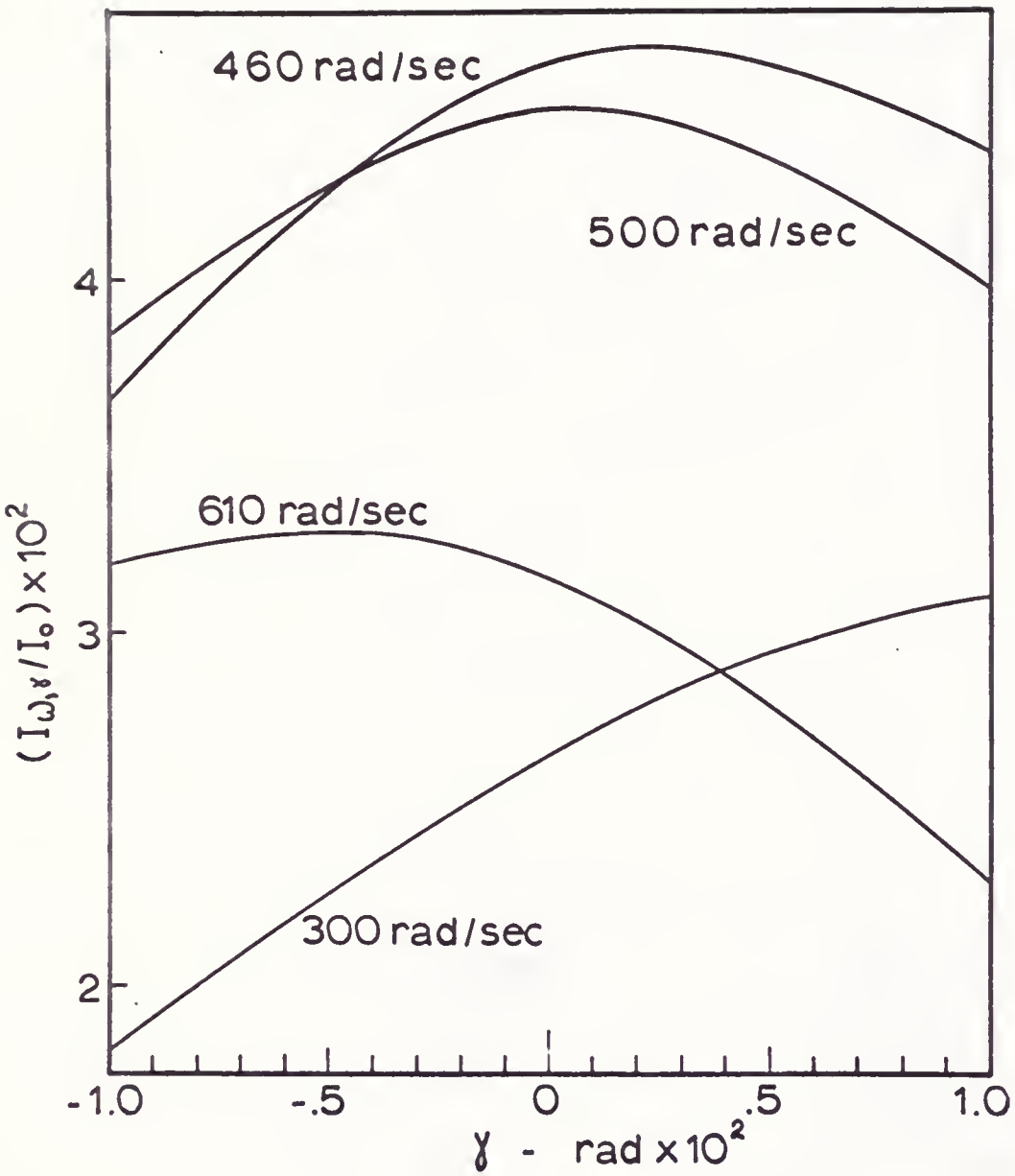
460 rad/sec
500 rad/sec
610 rad/sec
300 rad/sec
4
3
2
$(I_{\omega,\gamma}/I_o) \times 10^2$
-1.0
-.5
0
.5
1.0
γ - rad $\times 10^2$

on the low and high velocity sides of the distribution, respectively. The solid lines in Figure 24 are experimentally determined, and the dashed lines correspond to the calculated values of $I_{\omega,\gamma}$ assuming the absence of collimating apertures. The agreement between the theoretical and experimental values is seen to be good in the region where the detector is the umbra of the molecular beam.

In a manner similar to that used to obtain Eqn. (66), the narrow groove approximation to the attenuated transmitted intensity as a function of γ can be obtained;

$$I_{\omega,\gamma} = (I_o a n \rho_\gamma / R_1 \pi) X_B^4 \exp(-X_B^2) \exp[-\ell_\gamma' n_G \sigma \psi(X_G)/\pi^{1/2} X_G^2] \qquad (70)$$

where ρ_γ is the γ angular dependent resolution and ℓ' is the same as ℓ_γ' in Eqn. (60) with $\ell_{2,\gamma}$ being the linear distance from the entrance to the selector chamber to the detector at ϕ_γ . Figure 25 illustrates the dependence of on the incidence angle γ . The data for this plot were obtained from the intercepts of $\ln(I_{\omega,\gamma}/I_o\, \omega^4)$ versus ω^2 plots made for seven angular speeds in the range 200 to 600 rad./sec. Linear least square fits to these plots for ρ_γ produced straight lines with less than 0.03 per cent average deviations.

Fig. 24.-Comparison of measured values for angular dependence of narrow Maxwellian beam with those calculated for beam with no collimation.

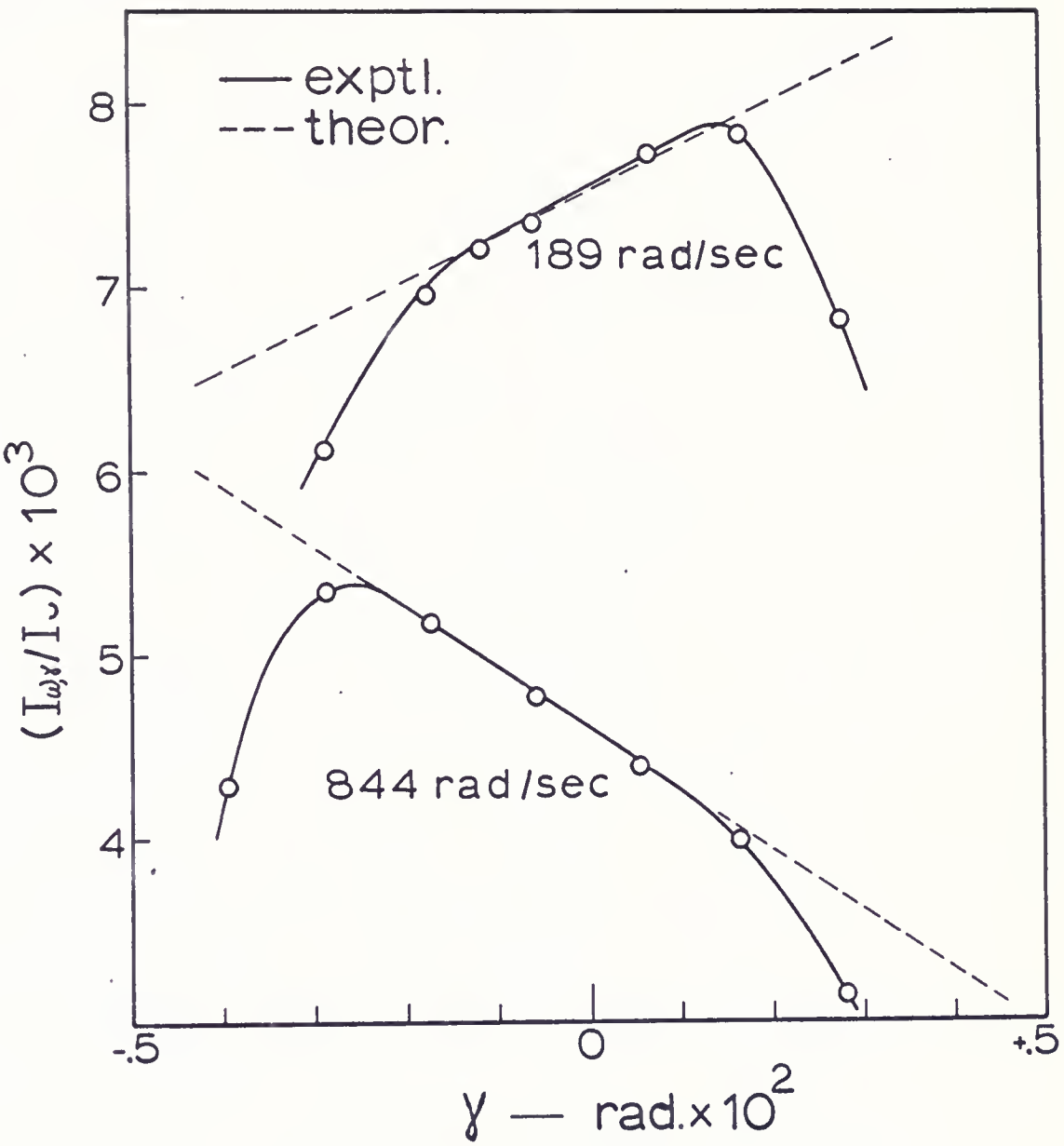
exptl.
theor.
189 rad/sec
844 rad/sec
8
7
6
5
4
-.5
0
+.5
$(I_{\omega\gamma}/I_\omega) \times 10^3$
γ — rad.$\times 10^2$

Fig. 25.-Plot of resolution versus angle of incidence for the velocity selector with the parameters of Table 3.

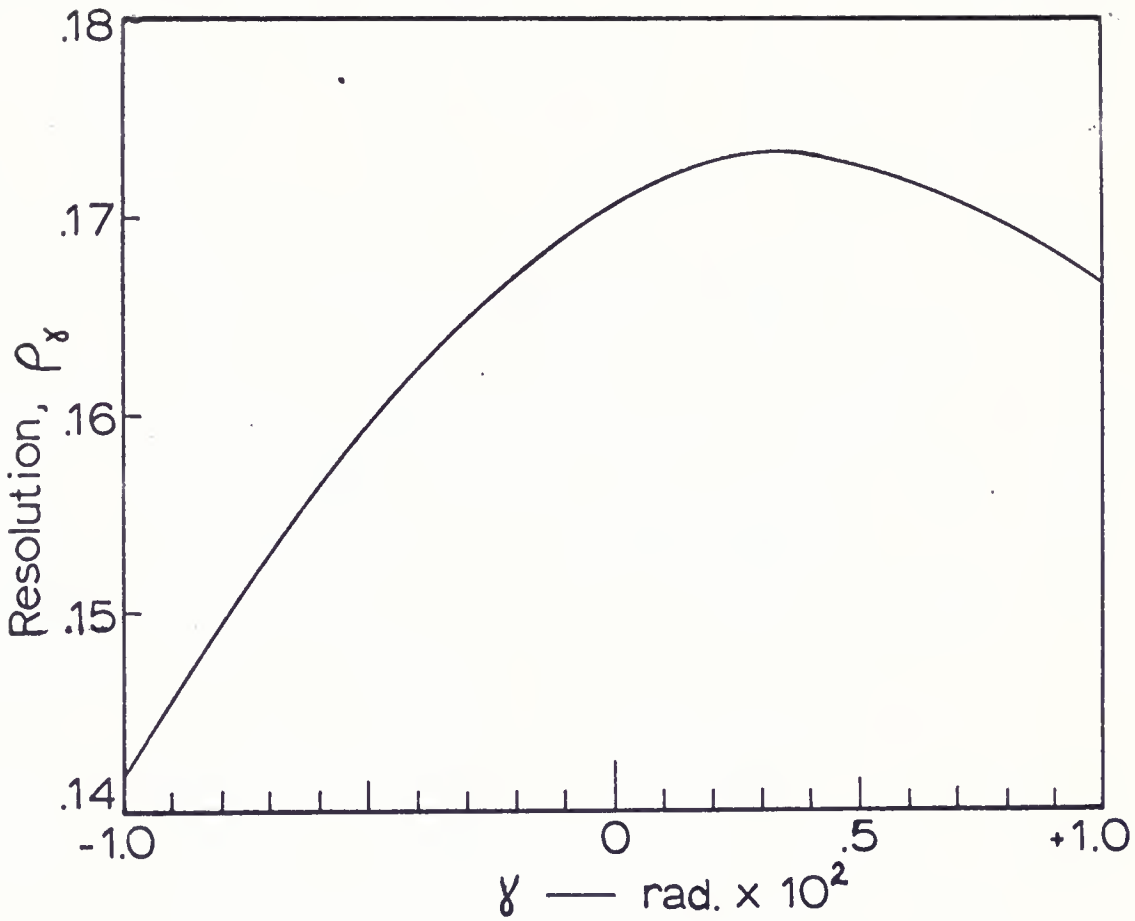
.18
.17
.16
.15
.14
Resolution, ρ_γ
-1.0
0
.5
+1.0
γ — rad. x 10^2

B. Cross-Sections

According to the procedure previously outlined, total cross-sections for the scattering of cesium by argon and nitrogen in the thermal energy range were determined. However, before any consideration is given to the results, the angles through which scattering can be detected should be mentioned. For the experimental conditions listed in Table 2 the resolution for the apparatus, using the Kusch[51] 50 per cent criterion, is 3 min. This resolution is the minimum scattering angle for which the probability of detection is 50 per cent. It is interesting to note that less than 20 per cent of the particles scattered through an angle of 6 min. will reach the detector.

The expression used to relate the unattenuated and attenuated transmitted beam intensities (I_o and I respectively), at a particular angular speed of the velocity selector to the total cross-section is derived in Appendix II. The relative velocity dependent cross-sections for the Cs - Ar and Cs - N_2 systems are depicted in Figures 26 and 27, respectively, the average relative velocities being computed by considering the mean velocity, v_M, transmitted by the selector (at a particular angular speed) and the Maxwellian distributions of velocities present in the scattering gas. (It should be noted that these cross-sections were compared to those obtained using the Berkling

Fig. 26.-Average relative velocity dependent total cross-sections for Cs - Ar.

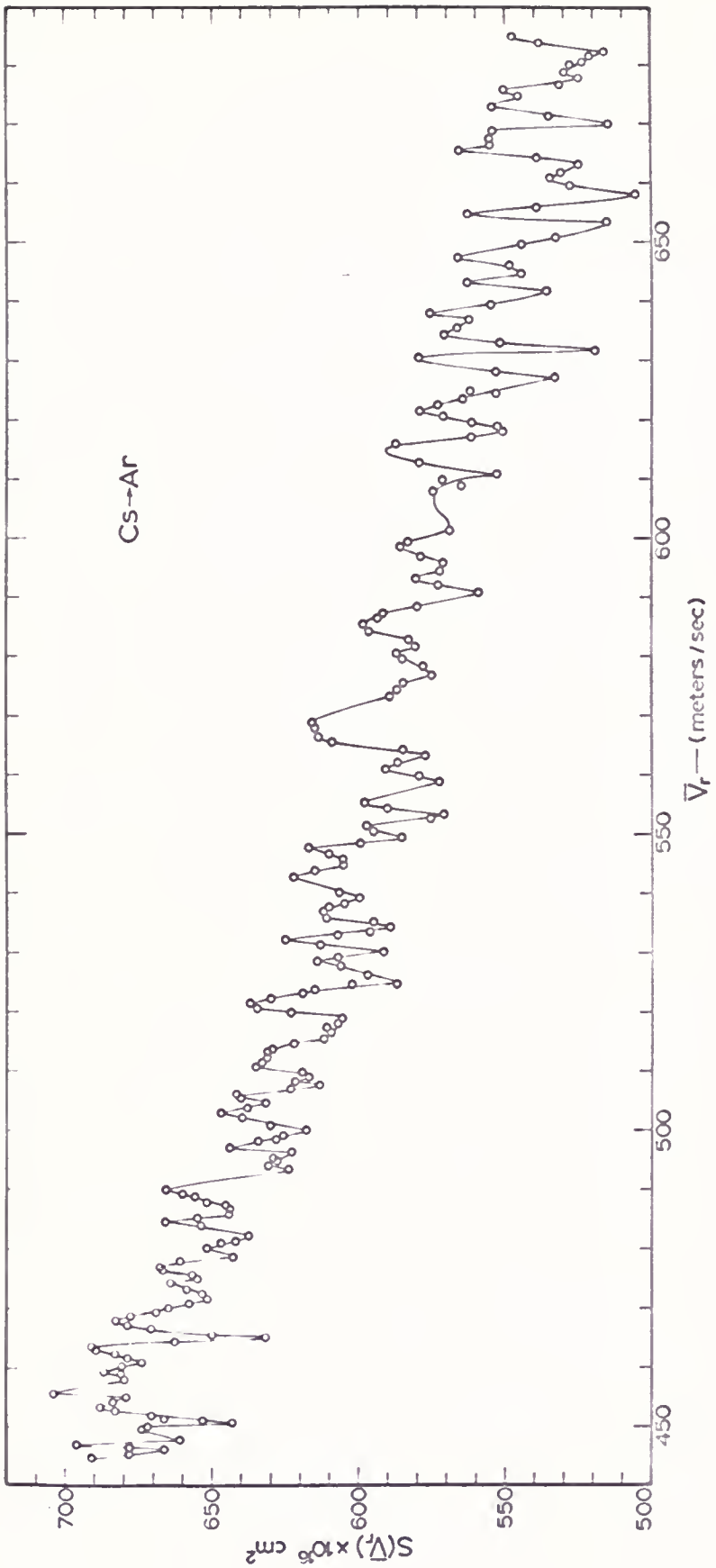
Cs-Ar
$S(\bar{V}_r) \times 10^{16}$ cm^2
700
650
600
550
500
450
500
550
600
650
$\bar{V}_r$ — (meters/sec)

Fig. 27.-Average relative velocity dependent total cross-sections for Cs - N_2.

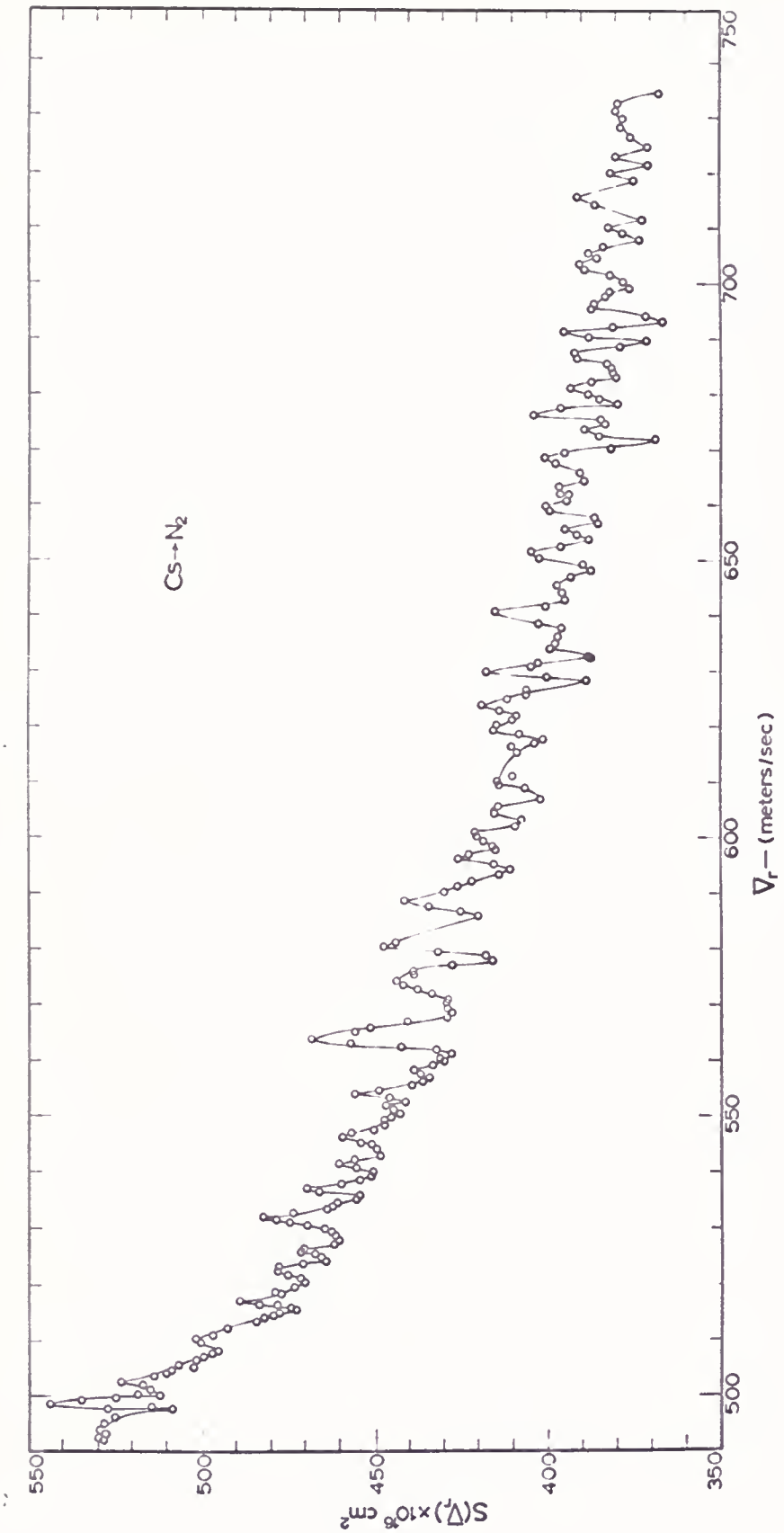
Cs→N2
S(V_r)×10^8 cm^2
V_r — (meters/sec)
550
500
450
400
350
500
550
600
650
700
750

functions[52] for n = 6; the agreement was within 1 per cent when corresponding physical situations were considered.) Figures 26 and 27 demonstrate the expected increase in cross-section with a corresponding reduction in the average relative velocity; however, an interesting and unexpected feature of these plots is their undulatory behavior. It can be seen that for both systems there appears to be more than just a random distribution associated with the fluctuations. It will also be noted that the periods of the undulations increase as the average relative velocity is reduced. An explanation for this unusual behavior is not easily found. The most reasonable one would attribute these fluctuations to some artifact of the apparatus. This was considered and measurements were taken under widely varying conditions; all resulting in the continued presence of the undulations. A partial explanation may lie in uncertainty of the determination of the $\ln (I_0/I)$. It is estimated that both I and I_0 can be measured within 1 per cent; for the attenuation used ($\sim$ 30 per cent) this error in intensities results in a 7 per cent possible error in the $\ln(I_0/I)$. Although this could explain the fluctuations seen in the cross-sections, it should not impart any regularity to them. It can be said at this time only that the origin of these undulations is not known and they will be the subject of further investigation.

From Eqn. (52) it is seen that if (in this energy range) a interatomic potential of the form

$$V(r) = C/r^s \text{ for } s \geq 3$$

is applicable, a plot of the $\ln[S(v_r)]$ versus $\ln v_r$ should produce a straight line whose slope is $-2/(s-1)$. When plots such as this are made and a linear least square fit applied to them, slopes obtained for the Cs - Ar and Cs - N_2 systems are $-.58 \pm .1$ and $-.55 \pm .1$, respectively, with the rather large deviations arising from the fluctuations in the cross section. An interesting feature of the above plot for the Cs - N_2 system is the marked change in slope for average relative velocities below 520 m/sec. This is probably an indication of some inelastic collisional contribution to the total cross-section. The appearance of a maximum in Figure 22 is also suggestive of an inelastic contribution to the cross-section in this energy range. At present no explanation for this occurrence is available.

If the intermolecular potentials for Cs - Ar and Cs - N_2 are assumed to be of the form $V(r) = -C/r^6$ then the potential constants can be evaluated from the Landau-Lifshitz formula (Eqn. 52) where

$$C = 5.676 \times 10^{-30} V_r [S(v_r)]^{5/2} \qquad (71)$$

a value of C is calculated for each S, and the individual

values are averaged. These parameters given in Table 4 along with available theoretical values and also values calculated from other thermal beam scattering experiments (non-velocity selected).

As can be seen from Table 4, excellent agreement is obtained between the measured value for Cs - Ar and the theoretical value calculated by Dalgarno. Unfortunately there does not exist a theoretical value for Cs - N_2 intermolecular potential constant.

A total reliability of $\pm$ 10 per cent is placed on the cross-sections reported. The uncertainties are of two kinds: uncertainty in the number density of scattering gas particles and in the beam intensities. A 3 per cent uncertainty has been assigned to the number density; while the uncertainty associated $\ln(I_0/I)$ has already been placed at 7 per cent. The possibility of the introduction of appreciable error due to the effects of angular resolution of the apparatus was considered. This may be estimated by the expression[53]

$$\Delta S = 0.027 S^2 k^2 \chi \qquad (72)$$

where χ is the resolution and k the wave number of the beam particle. The resulting error is less than 1 per cent; so this resolution effect was ignored.

Table 4.--Interatomic Potential Constants for Cesium (in units of 10^{-58} erg. cm^6).

Scattering Gas	Relative Velocity Range	C Present Experiment	C Theoretical	C Other Experiments
Ar	440-690 m/sec.	2.80	3.0_5[a]	6.2[b]
				4.0[c]
N_2	490-740 m/sec.	1.37		5.9[d]
				6.1[b]

[a] A. Dalgarno and A. E. Kingston, Proc. Phys. Soc. 73, 455 (1959).

[b] E. W. Rothe and R. B. Bernstein, J. Chem. Phys. 31, 1619 (1959).

[c] See Ref. 17.

[d] See Ref. 12.

C. Concluding Remarks

The excellent agreement between the theoretical and observed transmission characteristics of the velocity selector acting on a Maxwellian beam illustrates the utility of this selector for determining the velocity distributions of a beam generated under non-ideal conditions. Such beams are desirable because of high-intensity or high velocity characteristics, and although they are used extensively in many phases of molecular beam research, very little experimental information concerning them is available. The most important aspect of the detailed analysis of transmission characteristics is the ability to determine intensity and velocity distributions of molecules arriving at the scattering zone, thus permitting precise interpretation of scattering measurements on simultaneous velocity selected molecular beams.

For the low energy alkali metal-inert gas interatomic potential constants (assuming $V(r) = C/r^6$) a discrepancy has always existed between the experimental and theoretical values. It is believed that this discrepancy has resulted in part from the persistent inaccurate determination of the number density of scattering particles along the beam path. For the present work it is felt that measurement of the scattering gas pressure by means of a gauge located in the scattering chamber and treatment of target-gas densities

along the beam path (Appendix II) allows the most accurate determination of cross-sections made thus far. Support is given to the theoretical potential constant for the Cs - Ar system by its close agreement with the value obtained from this experiment. (It should be noted that an error of 10 per cent in S will produce a 28 per cent error in C.) Further determinations of alkali metal-inert gas cross-section are called for to provide further tests of the present technique. If agreement with theory persists, it seems likely there will accrue from these studies a reliable value of the long awaited "absolute" cross-section in terms of which the numerous available relative cross-sections may be deduced.[54]

APPENDICES

APPENDIX I

SCATTERING GAS PRESSURE MEASUREMENT

A thermocouple vacuum gauge consists of a heated wire to the center of which is attached a fine thermocouple whose reference junction is at the temperature of the enclosure. The range of pressures over which a gauge of this type may be used is roughly 0.1-100 microns. In general the temperature of the junction is dependent on: the power supplied to the heater, the pressure of the gas, the accommodation coefficient of gas on the surface of the heater wire, and the thermal conductivity. Consequently, the output of the thermocouple is a function of the ambient temperature of the gauge, the type and density of the gas, and the power supplied the heater. For the use of this gauge in precise measurements of pressure of a particular gas the usual practice is to fix the heater current and obtain calibration curves over the anticipated ambient temperature range, then, if possible, to express the pressure as a function of the thermocouple output and ambient temperature. All experimental measurements using this gauge must then be made with the heater current exactly the same as used in calibration. This procedure is

somewhat cumbersome and can give rise to considerable problems; however, it has been found that a plot of $(E_o - E)/E_o$ versus p (where E_o is the output of the gauge under high vacuum and E is the output at pressure p) for a particular gas is independent of the ambient temperature and the heater current. Therefore, if the gauge is calibrated at one temperature and heater current in this manner subsequent use of the gauge need not correspond exactly to the calibration conditions. The various calibrations of this type (0.5-5 microns range) over an ambient temperature range of 25-50°C and heater currents of 59-61 ma. differed by only 1.5 per cent.

APPENDIX II

CALCULATION OF TOTAL CROSS-SECTION

Before an evaluation of the total cross-section can be made, the number density of scattering gas molecules at all positions along the beam path must be determined. There are three regions over which this density should be considered: the scattering chamber, slit channel, and outside the scattering chamber. For the present experiment the slit channel region is neglected because of its short length (0.002 in.). In the region outside the scattering chamber the density has two sources: that arising from the general increase in the background due to gas being present in the scattering chamber, and that arising from molecules effusing directly from the slits of the scattering chamber prior to colliding with walls of the apparatus. The rise in background pressure (upon introduction of gas into the scattering chamber) is directly measured; however, along the beam path the number density of the scattering gas inside of or emanating from the scattering chamber must be computed.

For the present experiment the pressure of the gas in the scattering chamber is such that the mean free path of these molecules is extremely large compared to any

dimension of the chamber. Therefore, the vast majority of collisions in the gas are with the chamber walls; so that the gas can be considered to radiate from these walls with a Maxwellian distribution of velocities. Considering only the scattering gas which does not constitute background, if P is any point along the beam path and Q is a point in the scattering chamber from which the slits can not be seen; then by the cosine law of radiation[55] the ratio of the number density of P to the number density at Q is equal to the ratio of the solid angle substended at P by the exposed inner surface of the scattering chamber to the solid angle 4π. The location of the thermocouple gauge within the scattering chamber is such that it can see only an infinitesimal portion of the total slit area; thus this gauge may be used to measure the number density at a point such as Q mentioned above. A coordinate system is now set up with its origin at the center of the scattering chamber such that the z-axis is along the central beam axis and the x-axis perpendicular to the plane of the beam. For rectangular slit geometry where a is the half width, b the half length, and ρ_m the half length of the diagonal the solid angle subtended at a point outside the scattering chamber by the front slit is

$$W_f(x,y,z) = 4\ \cos^{-1}(a/\rho_m) - \sin^{-1}[(z-\ell_s/2)(\rho_m^2 - a^2)^{1/2}/(a^2 + (z-\ell_s/2)^2)^{1/2}\rho_m] x(z-\ell_s/2)/[(z-\ell_s/2)^2 + x^2 + y^2]^{1/2}\ , \tag{73}$$

and by the back slit

$$W_b(x,y,z) = 4\ \cos^{-1}(a/\rho_m) - \sin^{-1}[(z+\ell_s/2)(\rho_m^2 - a^2)^{1/2}/(a^2 + (z+\ell_s/2)^2)^{1/2}\rho_m] x(z+\ell_s/2)/[(z+\ell_s/2) + x^2 + y^2]^{1/2}\ , \tag{74}$$

where ℓ_s is the distance between the slits. The number density at the point (x,y,z) is then

$$n(x,y,z)_o = n_{SG}[W_f - W_b]/4\pi\ , \tag{75}$$

where n_{SG} is the number density in the vicinity of the thermocouple gauge. For any point in the beam path within the scattering chamber the solid angles w_1 and w_2 substended by the slits are obtained by substituting z and $z - \ell$ for $(z \pm \ell_s/2)$ in Eqns. (73) and (74); therefore the number densities at these points are given by

$$n(x,y,z)_i = n_{SG}[1-(w_1 + w_2)]/4\pi\ . \tag{76}$$

Figure 28 is a plot of relative densities along the central beam axis. The function describing the scattering gas density at any position along the beam path has a minimum at the center of the beam. For this experiment the average

Fig. 28.-Relative scattering gas density along central beam axis (neglecting slit channel region).

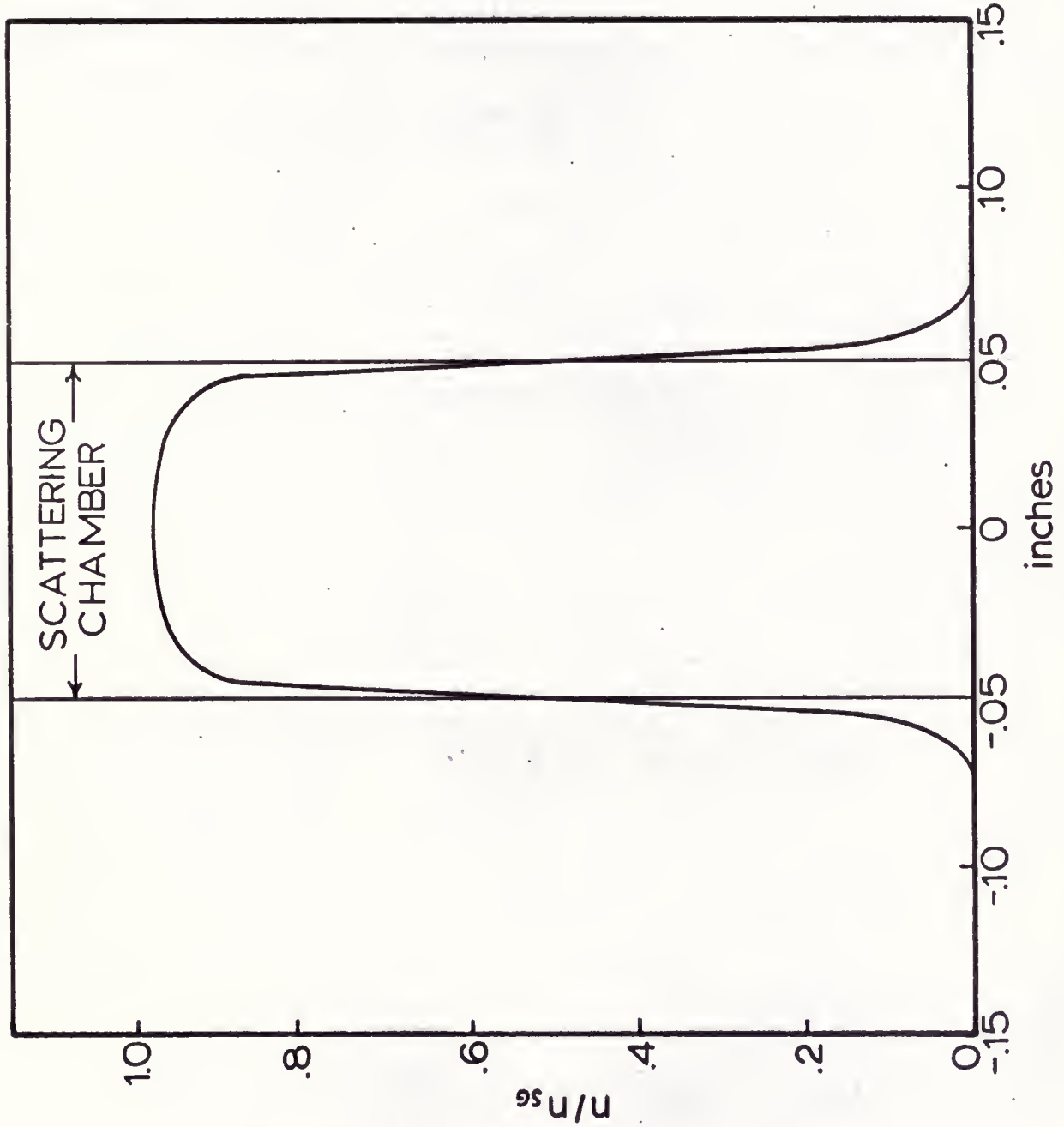
SCATTERING CHAMBER
n/n_sg
1.0
.8
.6
.4
.2
0
-.15
-.10
-.05
0
.05
.10
.15
inches

relative density, D_{SG}, in the beam path with the scattering chamber is .986. The integral

$$F = \int (n(o,o,z)_i/n_{SG})dz \qquad (77)$$

was evaluated numerically over the limits $\ell_s/2$ to 2 in. (at 2 in. $n(o,o,z)/n_{SG} = 1 \times 10^{-6}$) and found to be 0.0118; this was taken as the average number of scattering gas molecules (relative to n_{SG}) effusing from a slit and within the volume swept out by the beam.

Having now determined the scattering gas density at all positions along the beam path, the cross-section may be evaluated.

The probability that a beam molecule of velocity v_B traverse the distance between the source and detector without undergoing scattering is given by

$$P(v_B) = \exp[\sum_i \ell_i / \lambda(v_B)_i] \quad , \qquad (78)$$

where ℓ_i is the distance the molecule traverses while its mean free path is $\lambda(v_B)_i$. The scattering gas in the background and scattering chamber has Maxwellian velocity distributions so that the mean free path (see Eqn. 63) is given by

$$\lambda(v_B) = (v_B\pi/\alpha_{SG})^2/nS\psi(v_B/\alpha_{SG}) \quad , \qquad (79)$$

where α_{SG} is the most probable speed of the scattering gas, S is the total cross-section, and n is the scattering gas

number density (n_{BG} for the background and D_{SG} for the scattering chamber).

The evaluation of the mean free path of a beam molecule moving through gas effusing from the scattering chamber requires the average velocity between the beam and target molecules. The velocity distribution function of a Maxwellian beam (Eqn. 55) is given by

$$f(v) = 2\beta^4 v^3 \exp(\beta^2 v^2) \quad , \tag{80}$$

where $\beta^2 = m/2kT = 1/\alpha_{SG}^2$. Considering only those molecules whose trajectories are very nearly parallel to the beam, the average relative velocity is given by

$$\bar{v}_r = \int_0^\infty f(v)(v_B \pm v)dv = v_B \pm 3\pi^{1/2}/4\alpha_{SG} \quad , \tag{81}$$

where $\bar{v}_{r_1} = v_B - 3\pi^{1/2}/4\alpha_{SG}$ is in the region between the beam source and scattering chamber and $\bar{v}_{r_2} = v_B + 3\pi^{1/2}/4\alpha_{SG}$ is in the region between the scattering chamber and detector. The mean free path is given by

$$\lambda(v_B) = v_B(L - \ell_s/2)/FS\bar{v}_r \quad , \tag{82}$$

where $L - \ell_s/2$ is the range over which F has been evaluated.

Using the various $\lambda(v_B)$'s obtained above and Eqn. (78) there results

$$I = I_o \exp \left\{ n_{SG} F(\bar{v}_{r_1} + \bar{v}_{r_2}) S/v_B + S[\psi(v_B/\alpha_{SG}) / (v_B\pi/\alpha_{SG})^2] \times [\ell_s D_{SG} + (\ell_o + \ell_d) n_{BG}] \right\} \quad (83)$$

where ℓ_o and ℓ_d are the distances between the source and scattering chamber and between the scattering chamber and detector, respectively. From Eqn. (81) $\bar{v}_{r_1} + \bar{v}_{r_2} = 2v_B$ so that Eqn. (83) can be written in the form

$$S = (\ln I_o/I) / \left\{ 2n_{SG} F + [\psi(v_B/\alpha_{SG})/(v_B\pi/\alpha_{SG})^2] \times [\ell_s D_{SG} + (\ell_o + \ell_d) n_{BG}] \right\} \quad (84)$$

Cross-sections calculated in this manner are functions of the average relative velocity between the beam molecule and scattering gas so that S should be written as $S(v_r)$.

REFERENCES

1. Herschfelder, Curtiss, and Bird, Molecular Theory of Gases and Liquids (John Wiley and Sons, Inc., New York, 1954), Chap. 1, 12, and 13.

2. In general the term molecule is used with the intention of denoting atoms as well.

3. I. Amdur and H. Pearlman, J. Chem. Phys. 8, 7 (1940).

4. I. Amdur, E. A. Mason, and J. E. Jordan, J. Chem. Phys. 27, 527 (1957).

5. I. Amdur, J. E. Jordan, and S. O. Colgate, J. Chem. Phys. 34, 1545 (1961).

6. F. London, Trans. Faraday Soc. 33, 8 (1937).

7. R. D. Present, Kinetic Theory of Gases (McGraw-Hill Book Company, Inc., New York, 1958), p. 244.

8. Herschfelder, Curtiss, and Bird, op. cit., p. 207.

9. I. Estermann, Rev. Mod. Phys. 18, 300 (1946).

10. L. Dunoyer, Comptes rendus 152, 594 (1911).

11. O. Stern, Z. Physik 2, 49 (1920).

12. H. Pauly, Z. angew. Physik 9, 600 (1957).

13. K. Kodera and T. Tamura, Bull. Chem. Soc. Japan 34, 566 (1961).

14. R. C. Schoonmaker, J. Phys. Chem. 65, 892 (1961).

15. P. K. Rol and E. W. Rothe, Phys. Rev. Letters 9, 494 (1962).

16. E. W. Rothe, P. K. Rol, and R. B. Bernstein, Phys. Rev. 130, 2333 (1963).

17. R. Helbing and H. Pauly, Z. Physik 179, 16 (1964).

18. H. S. W. Massey and C. B. O. Mohr, Proc. Roy. Soc. A144, 188 (1934).

19. J. L. Costa, H. D. Smyth, and K. T. Compton, Phys. Rev. 30, 349 (1927).

20. V. W. Cohen and A. Ellett, Phys. Rev. 52, 502 (1937).

21. I. Estermann, O. C. Simpson, and O. Stern, Phys. Rev. 71, 238 (1947).

22. J. G. Dash and H. S. Summers Jr., Rev. Sci. Instr. 24, 91 (1952).

23. R. C. Miller and P. Kusch, Phys. Rev. 99, 1314 (1955).

24. E. F. Green, R. W. Roberts, and J. Ross, J. Chem. Phys. 32, 940 (1960).

25. H. G. Bumnewitz and W. Paul, Z. Physik 139, 489 (1954).

26. S. V. Hostettler and R. B. Bernstein, Rev. Sci. Instr. 31, 872 (1960).

27. S. M. Trujillo, P. K. Rol, and E. W. Rothe, Rev. Sci. Instr. 33, 841 (1962).

28. K. Lulla, H. Brown, and B. Bederson, Phys. Rev. 136, 1233 (1964).

29. J. L. Kinsey, Rev. Sci. Instr. (to be published).

30. G. Becker, Z. angew. Physik 13, 59 (1961).

31. J. Deckers and J. B. Fenn, Rev. Sci. Instr. 34, 96 (1963).

32. A. E. Grosser, R. P. Iczkowski, and J. L. Margrave, Rev. Sci. Instr. 34, 116 (1963).

33. Two phase four pole hysteresis syncronous motor, model CP34HD86 McLean Syntorque Corp.

34. S. O. Colgate, Rev. Sci. Instr. 34, 771 (1963).

35. Stainless steel, single edge, injector Pal razor blades were used.

36. 15 watt, 115 volts Hotwatt model SC 121.

37. I. Langmuir and K. H. Kingdon, Proc. Roy. Soc. A107, 61 (1925).

38. J. B. Taylor, Z. Physik 57, 242 (1929).

39. S. Datz and E. H. Taylor, J. Chem. Phys. 25, 389 (1956).

40. The 0.003 in. diameter tungsten wire is drawn from a single crystal and was furnished by D. R. Herschbach.

41. S. O. Colgate and T. C. Imeson, Rev. Sci. Instr. 36, 932 (1965).

42. E. H. Kennard, op. cit., Chap. 3.

43. D. Bohm, Quantum Theory (Prentice-Hall, Inc., Englewood Cliffs, N.J., 1951), Chap. 21.

44. L. D. Landau and E. M. Lifshitz, Quantum Mechanics (Addison-Wesley Publishing Co., Inc., Reading, Massachusetts, 1958), Chap. 14.

45. L. I. Schiff, Quantum Mechanics (McGraw-Hill Book Co., Inc., New York, N.Y., 1955), Chap. 5.

46. E. A. Mason, J. T. Vanderslice, and C. J. C. Raw, J. Chem. Phys. 40, 2153 (1964).

47. The notation y indicates the derivative of the function y taken with respect to time.

48. N. F. Ramsey, Molecular Beams (Oxford University Press, London, 1956), p. 20.

49. The error function was calculated using the closed form approximation given in: C. Hastings Jr., Approximations for Digital Computers (Princeton University Press, Princeton, New Jersey, 1955), p. 187.

50. E. H. Kennard, op. cit., p. 108.

51. P. Kusch, J. Chem. Phys. 40, 1 (1964).

52. K. Berkling, R. Helbing, K. Kramer, H. Pauly, C. Schlier, and P. Toschek, Z. Physik 166, 406 (1962).

53. H. Pauly, Z. Physik 157, 54 (1959).

54. R. B. Bernstein, Atomic Collision Processes (North-Holland Publishing Co., Amsterdam, 1964), p. 895.

55. W. J. Taylor, J. Chem. Phys. 38, 779 (1963).

V I T A

Thomas Cole Imeson II was born in Jacksonville, Florida on November 29, 1938. After attending elementary and secondary school in the Duval County School System, he attended Washington and Lee University in Lexington, Virginia, from which he received the B.S. degree in Chemistry in June, 1961. Since September, 1961, he has been enrolled in the Graduate School of the University of Florida studying for the Ph.D. degree.

This dissertation was prepared under the direction of the chairman of the candidate's supervisory committee and has been approved by all members of that committee. It was submitted to the Dean of the College of Arts and Sciences and to the Graduate Council, and was approved as partial fulfillment of the requirements for the degree of Doctor of Philosophy.

December 18, 1965

E. Ruffin Jones
Dean, College of Arts and Sciences

Dean, Graduate School

Supervisory Committee:

S. O. Colgate
Chairman

E E Muschlitz, Jr.

R. D. Dresdner

T. L. Bailey

J. O. Moore